PEPPERDINE UNIVERSITY

Pepperdine University
Pepperdine Digital Commons

Featured Research | Undergraduate Student Research

2-7-2014

Delivery and Pitch Type Alter Ground Reaction Forces in Baseball Pitching

Garrett Kass
Pepperdine University

Follow this and additional works at: https://digitalcommons.pepperdine.edu/sturesearch

 Part of the Sports Sciences Commons

Recommended Citation

Kass, Garrett, "Delivery and Pitch Type Alter Ground Reaction Forces in Baseball Pitching" (2014). Pepperdine University, *Featured Research.* Paper 78.
https://digitalcommons.pepperdine.edu/sturesearch/78

This Senior Thesis is brought to you for free and open access by the Undergraduate Student Research at Pepperdine Digital Commons. It has been accepted for inclusion in Featured Research by an authorized administrator of Pepperdine Digital Commons. For more information, please contact bailey.berry@pepperdine.edu.

DELIVERY AND PITCH TYPE ALTER GROUND REACTION FORCES IN BASEBALL PITCHING

Garrett Kass

Natural Science Division

Pepperdine University

Malibu, CA 90263

Submitted in Partial Fulfillment of the Requirements for

Graduation with Honors in Sports Medicine

Pepperdine University
Seaver College

February 7, 2014

WE HEREBY RECOMMEND THAT THE THESIS BY

Garrett Kass

ENTITLED Delivery and Pitch Type Alter Ground Reaction Forces in Baseball Pitching

BE ACCEPTED IN PARTIAL FULFILLMENT OF THE REQUIREMENTS FOR HONORS IN SPORTS MEDICINE

Dean of Seaver College

Head of Division

Honors Thesis Chairperson

Honors Thesis Committee

Dr. Michael E. Feltner, Chair

Dr. Cooker Storm

Dr. David Strong

Dr. Terry Kite

Dr. Gerwyn Hughes

Professor Lex Gidley

Introduction

Background and Concepts

The biomechanics of the overhand throwing motion of baseball pitchers has been studied by many scholars for over 50 years with important studies being done by Atwater (1970), Feltner (1986), and Fleisig (1989). These first few studies were crucial in establishing the foundation for kinematic and kinetic analysis of overhead throwing. From there, studies such as Feltner (1986), Dillman (1993) and Lin (2003) have shown baseball pitching to result from the sequential coordinated segmental rotations of body segments that ultimately result in a large force applied to the baseball. In turn, this force produces a large velocity of the ball at release. Yet, few scholars have investigated the ground reaction forces that produce the rotation of the body segments and ultimately are responsible for the production of the force applied to the ball.

This study is important because pitchers are coached to use their legs to create ground reaction forces that will help them produce a greater ball speed when pitching; however, more evidence is required to detail the underlying performance theory. Previously published studies by Elliott (1988), Feltner (1986), and MacWilliams (1998), have shown that there is a transfer of angular momentum through the body segments and that this angular momentum is created as a result of the ground reaction forces from the pitcher's feet. Thus, these studies were foundational to our research question and project.

The angular momentum (H) of the pitcher about the axes through his center of mass (g) at release results from the integral of the sum torques exerted about g from the start of the pitching motion (H = 0) to ball release. From Newton's Second Law, we learn

$$\sum \overrightarrow{T_g} = {}^{d\vec{H}}/_{dt} \tag{1}$$

or

$$\int_{t_{start}}^{t_{release}} \sum \overrightarrow{T_g}\,(t) = \Delta\, \vec{H}_{release/start} = \vec{H}_{release} - \vec{H}_{start} \tag{2}$$

where t_{start} is the instant immediately before the pitcher begins his motion (i.e. when H_{START} = 0). Therefore, equation (2) becomes

$$\int_{t_{start}}^{t_{release}} \sum \overrightarrow{T_g}\,(t) = \vec{H}_{release} \tag{3}$$

A free body diagram of a pitcher at any point in the pitch is shown in Figure 1.

Figure 1. Free body diagram of pitcher (Allison, 2008)

Three external forces ($\vec{F}_{\text{Left}}$, $\vec{F}_{\text{Right}}$, and $\vec{w}$) are being applied to the pitcher. $\vec{F}_{\text{Left}}$, $\vec{F}_{\text{Right}}$ are the ground reaction forces (GRFs) resulting from the actions of the pitcher's feet against the ground and $\vec{w}$ is the weight of the pitcher.

The torques created by each force about g are noted in the following equations:

$$\vec{T}_{Left} = \vec{r}_L \times \vec{F}_{Left} \quad (4)$$

$$\vec{T}_{Right} = \vec{r}_R \text{ x } \vec{F}_{Right} \quad (5)$$

$$\vec{T}_w = 0 \text{ x } \vec{w} = 0 \quad (6)$$

Where $\vec{r}_L$ and $\vec{r}_R$ are displacement vectors extending from g to the point of application of the two ground reaction forces, respectively. Thus, the angular momentum of the pitcher can be expressed as the sum of the integral of the torques produced by the two ground reaction forces from t_{start} through $t_{release}$.

$$\int_{t_{start}}^{t_{release}} \vec{T}_{Left}(t) + \int_{t_{start}}^{t_{release}} \vec{T}_{Right}(t) = \vec{H}_{release} \quad (7)$$

Determination of $\vec{T}_{\text{Left}}$ and $\vec{T}_{\text{Right}}$ require the computation of the location of g at each instant of the pitch. However, the limitations of our motion capture system at the time the study was conducted prevented determination of the three-dimensional (3D) coordinates of the body landmarks at a sufficient sampling rate to adequately determine the location of g. While this precluded the computation of $\vec{H}_{release}$, the motions of most pitchers are very similar and this suggests that $\vec{r}_L$ and $\vec{r}_R$ also are likely to be similar for most pitchers. Thus, examination of the changes in $\vec{F}_R$ and $\vec{F}_L$ will likely yield important insights regarding angular momentum production.

As described above, two ground reaction forces ($\vec{F}_{\text{Left}}$ and $\vec{F}_{\text{Right}}$) create torques ($\vec{T}_{\text{Left}}$ and $\vec{T}_{\text{Right}}$) about g that ultimately produce the segmental rotations of the body. This segmental rotation begins with the motions of the legs and is transferred up and through the body until it ultimately reaches the hand where a large force is applied to the ball. This force produces the speed of the ball at release. Examining the differences in ground reaction forces for different types of pitch delivery (windup or stretch) and pitch type (fastball or changeup) will provide further insight into the biomechanics of the pitching motion.

Review of Literature

Elliott et al. (1988) examined ground reaction forces in only the push foot using a single force plate under the pitching rubber. In examining only the ground reaction forces under the push foot, they showed that the resultant ground reaction forces were similar between both slow-throwing and fast-throwing subjects, but that there was a significant difference in the timing of their peak resultant force. Larger resultant forces were recorded for the fast-throwing subjects at front-foot landing, whereas the slow-throwing subjects recorded larger resultant forces at the time the throwing arm was extended. This demonstrated that the ability for the subject to drive the body over a stabilized front leg was characteristic of the fast-throwing pitchers (Fastballs = 77.4 mph; Curveballs = 67.3 mph). However, as shown by the fastball speeds, the pitchers were

of suboptimal skill considering most collegiate/major league baseball pitchers throw between 85-95 mph.

MacWilliams et al. (1998) used a pitching mound with two multicomponent force plates to record the ground reaction forces generated by pitchers under both the push and landing feet. The authors found that greater resultant ground reaction forces resulted in a greater wrist velocity at release. Thus, they established a link between leg drive (the leg motions of the pitcher) and arm velocity. Further, they concluded that leg drive is an important aspect of the overhead throwing motion. However, there findings were limited because, like Elliott et. al. (1988), they used pitchers with suboptimal skills as shown by the low linear wrist velocity data at release (≈40-50 mph). Secondly, the pitching mound used did not allow for cleats to be worn. Finally, they only had 28 trials which could be analyzed and did not investigate differences in pitch type or pitch delivery.

Purpose

The proposed study seeks to understand the effects of pitch delivery and pitch type on ground reaction forces and ball speed in baseball pitching. We hypothesize that ground reaction forces will differ between pitch types and pitch deliveries and result in different ball velocities.

Methods and Materials

Subjects

Eight collegiate male baseball players of the 2010-2011 Pepperdine University men's baseball team (height, mean = 188.8 cm, s = 5.1 cm; body mass, mean = 89.4 kg, s = 7.4 kg; age, mean =19.5, s = 0.8) provided voluntary written informed consent and served as participants. Four pitchers were right-handed and four pitchers were left-handed.

Procedures

After following their respective normal pre-game warm-up, each pitcher threw maximal effort pitches from the indoor pitching mound. Pitchers threw two types of pitches, a fastball or a changeup. Fastballs, the primary baseball pitch, are maximal effort pitches thrown by the pitcher. Changeups, a secondary baseball pitch, are thrown at a slower velocity than the fastball in order to disrupt the timing of the batter. The pitches were thrown using the two typical forms of pitch delivery, the windup or the stretch. The windup is the primary delivery type for most pitchers and is utilized when there are no runners on base. The stretch, on the other hand, is utilized predominantly when runners are on base to prevent them from stealing a base (see Figure 2 and Figure 3 for visual diagrams). Pitch delivery and pitch type were randomized for

each trial. A total of 20 trials were collected for each pitcher, 5 trials for each pitch delivery and pitch type combination.

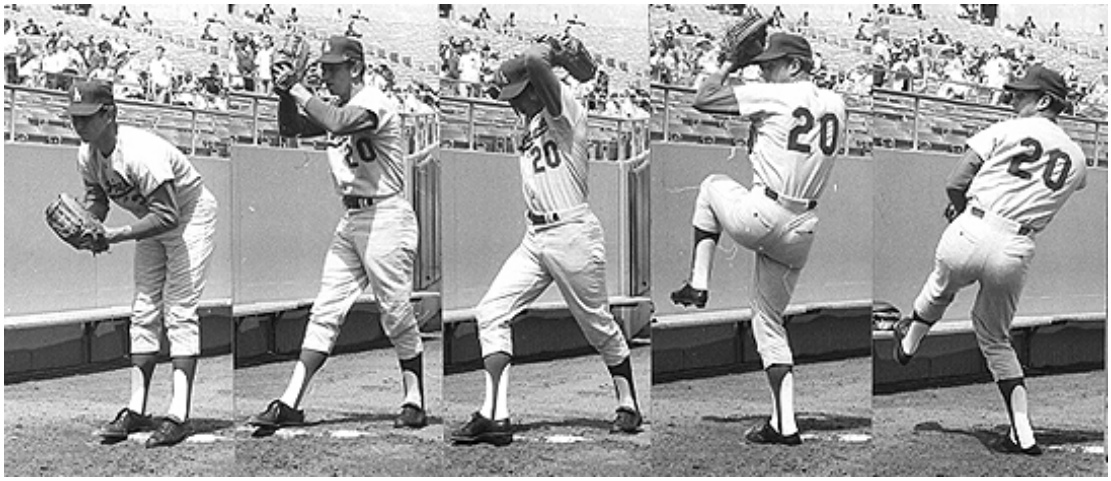

Figure 2. Time-lapse picture of the windup pitching motion (Weiskopf, 2012) [Chronologically left to right]

Figure 3. Time-lapse picture of stretch pitching motion (Bales, 2007) [Chronologically right to left]

Pitchers wore their normal metals baseball cleats for all trials. All pitches were thrown from a regulation Major League baseball pitching mound, having a slope of 1 inch per foot of length (2.54 cm per 30.48 cm of length), in which the force plates were embedded (Figures 4 and 5). For each trial, the pitchers threw a maximal effort pitch into a protective screen located 20 feet from the pitching rubber. After a pitcher finished all twenty trials, they followed their respective normal post-game cool-down routine.

Three types of data were collected for each trial. The ground reaction force data was collected using Kistler (Model No. 9281b) multicomponent force plates which were rigidly attached to the floor (Figure 4).

Figure 4. Kistler force plate setup prior to mound placement

Force Plate one (referenced as the Landing Plate) was installed into the floor using the standard Kistler 9281b floor installation. Force Plate two (referenced as the Rubber Plate) was mounted above the floor using a professionally fabricated mounting bracket. The indoor pitching mound was then modified to contain and conceal the two force plates. This allowed for collection of the GRF data from a pitching mound that appeared the same as a "normal" regulation pitching mound to the subjects (Figure 5).

Figure 5. Pitching mound installed over Kistler force plates.

Three-dimensional GRF data was sampled at a rate of 1200 Hz for each trial using Kistler Bioware software. The instants of stride leg lift and stride foot contact were also determined using the GRF data. Stride leg lift was the instant the GRF became zero on the rubber plate. Stride foot contact was determined as the instant the GRF became non-zero on the landing plate.

A standard video camcorder (60 Hz) was used to record the motions of the pitcher. Frame by frame analysis of the video was conducted using Virtualdub (Phaeron, 2010; http://www.virtualdub.org/) and used to determine the following instants:

1. Stride foot lift (t_{SFL}): the instant the stride foot left the surface of the rubber plate prior to stride foot contact
2. Stride foot contact (t_{SFC}): the instant the stride foot made contact with the landing plate prior to ball release
3. Push foot lift (t_{PFL}): the instant the push foot left the surface of the rubber plate after stride foot contact
4. Ball release (t_{REL}): the instant of ball release

The videotape recording also allowed the investigators to confirm that the stride foot of the pitcher landed fully on the surface of the landing plate. As the instants of stride leg lift and stride foot contact were determined using both the GRF and video data, the data obtained from the force plates could be then synchronized with the video data and the motions of the pitcher. Thus, the instant of ball release could be identified in the GRF data.

A radar gun (Jugs Pro-Sports Radar Gun) was used to determine the speed of each pitch. The radar gun was set up at an angle of 20 degrees from the line that runs perpendicular to the length of the pitching rubber through the center of home plate (the intended direction of the pitch). Ball speed in the direction of the pitch was then determined using the following equation:

$$Ball\ Speed = {Radar\ Speed}/{\cos(20°)}$$

Ball speeds recorded by the radar gun were accurate to within 0.25 m/s.

Data Processing

The reference coordinate system in which the ground reaction forces were recorded was the standard Kistler reference coordinate system ($R_{Kistler}$) shown in Figure 6:

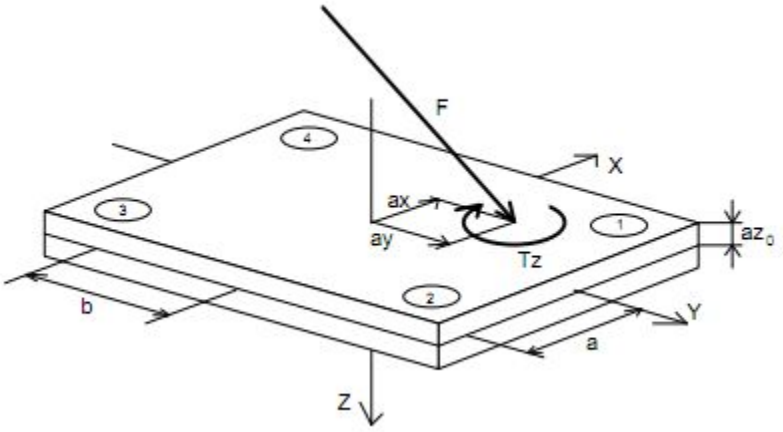

Figure 6. Standard Coordinate System of the Kistler Force Plates (Kistler, 2012).

The GRF data were then expressed in an activity-relevant reference frame ($R_{BASEBALL}$) and the forces were transformed to indicate the forces applied by the ground to the pitcher ($\vec{F}_{Left}$ and F_{Right}), not the forces applied by the pitcher to the force plate. In this reference frame, the Z direction was normal to the surface of the pitching mound and pointing upwards, the Y direction pointed directly towards home plate and the X direction pointed perpendicular to home plate and to the right of the pitching mound (Figure 7).

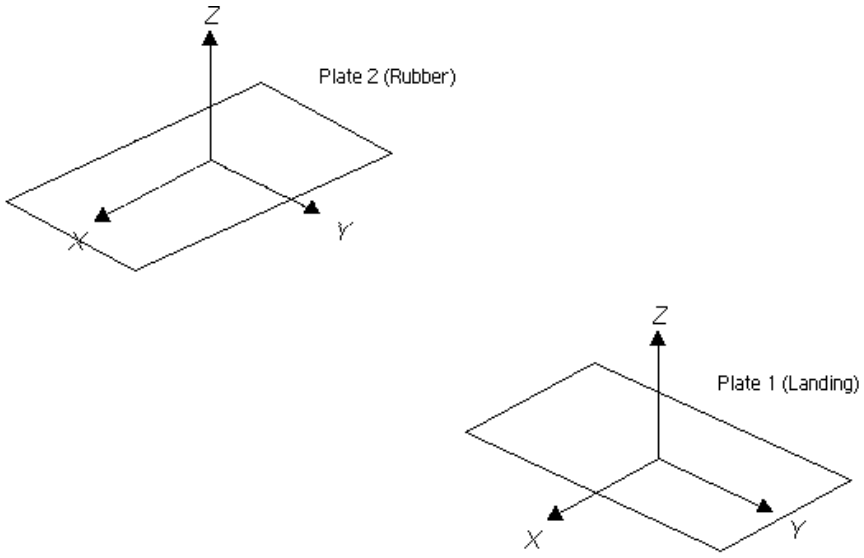

Figure 7. Post-transformation reference coordinate systems of the pitching mound force plates

Because the rubber plate was parallel with the floor, the reference frame is transformed from the Kistler reference frame to the activity relevant reference frame using the following translation matrix:

$$\begin{bmatrix} X(BASEBALL) \\ Y(BASEBALL) \\ Z(BASEBALL) \end{bmatrix} = \begin{bmatrix} 1 & 0 & 0 \\ 0 & -1 & 0 \\ 0 & 0 & 1 \end{bmatrix} \begin{bmatrix} X(Kistler) \\ Y(Kistler) \\ Z(Kistler) \end{bmatrix} \quad (8)$$

Note: X_1 in the translation matrix is negative for left-handed pitchers in order to treat their x-coordinate data as a right-handed pitcher.

For the landing plate, the Kistler reference frame is first translated to an intermediate reference frame using the following translation matrix:

$$\begin{bmatrix} X(Intermediate) \\ Y(Intermediate) \\ Z(Intermediate) \end{bmatrix} = \begin{bmatrix} 0 & -1 & 0 \\ -1 & 0 & 0 \\ 0 & 0 & 1 \end{bmatrix} \begin{bmatrix} X(Kistler) \\ Y(Kistler) \\ Z(Kistler) \end{bmatrix} \quad (9)$$

The landing plate also had to be corrected as the top surface of the pitching mound was inclined at an angle of 4.76º. To do this, a second reference frame transformation was necessary. The reference coordinate system was rotated to have the Z direction normal to the pitching mound. This was done using the following equation where theta is the 4.76º angle reflecting the slope of the pitching mound:

$$\begin{bmatrix} X(BASEBALL) \\ Y(BASEBALL) \\ Z(BASEBALL) \end{bmatrix} = \begin{bmatrix} 1 & 0 & 0 \\ 0 & \cos\Theta & \sin\Theta \\ 0 & -\sin\Theta & \cos\Theta \end{bmatrix} \begin{bmatrix} X(Intermediate) \\ Y(Intermediate) \\ Z(Intermediate) \end{bmatrix} \quad (10)$$

The center of pressure (the point of application of the resultant GRF on the surface of the mound) was calculated using the GRF data and corrected for plate padding. To correct for plate padding and correctly determine the location of the CP, the method described by Kwon (1998) was used.

To calculate the center of pressure, an understanding of how a force plate works is required. The force plate records the 3D forces acting on the plate at sensors located in each corner (Figure 6). The force data are then reported as a single 3D resultant ground reaction force ($\vec{F}$) and a free-torque vector ($\vec{T}_z$). The point of application of $\vec{F}$ is the center of pressure (CP). It is important to understand that in most force plates, the origin is not at the geometric center of the plate surface but rather is corrected by the manufacturer to a true origin labeled as (a, b, c) found in the calibration data sheet. This is shown in Figure 8.

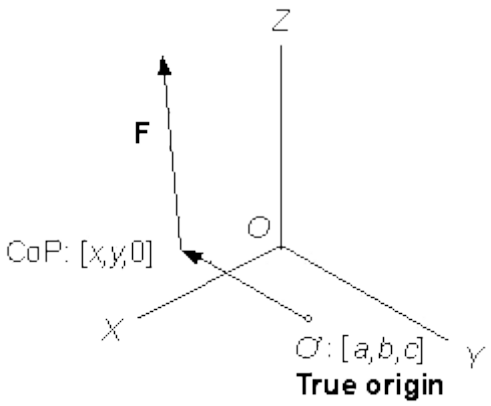

Figure 8. Center of Pressure about True Origin (Kwon, 2008)

To begin, the moment measured by the plate is equal to the moment created by $\vec{F}$ about the true origin and $\vec{T}_z$ as shown by equation (11).

$$\vec{M} = [x-a \quad y-b \quad -c] \text{ x } [F_x \quad F_y \quad F_z] + [0 \quad 0 \quad T_z] \tag{11}$$

Breaking equation (11) up into the components of the moment in each particular direction, we get equation (12).

$$\begin{bmatrix} M_x \\ M_y \\ M_z \end{bmatrix} = \begin{bmatrix} 0 & c & y-b \\ -c & 0 & -(x-a) \\ -(y-b) & x-a & 0 \end{bmatrix} \begin{bmatrix} F_x \\ F_y \\ F_z \end{bmatrix} + \begin{bmatrix} 0 \\ 0 \\ T_z \end{bmatrix} = \begin{bmatrix} (y-b)F_z + cF_y \\ -cF_x - (x-a)F_z \\ (x-a)F_y - (y-b)F_x + T_z \end{bmatrix} \tag{12}$$

In order to make it more relevant to the center of pressure, equation (12) can be algebraically manipulated to represent the X and Y coordinates of the center of pressure relative to the true origin as well as the free torque vector ($\vec{T}z$) as shown in equations (13a), (13b), and (13c), respectively.

$$\text{x} = \; - \frac{\vec{M}_y + c\vec{F}_x}{\vec{F}_z} + \; a \tag{13a}$$

$$\text{y} = \; \frac{\vec{M}_x - c\vec{F}_y}{\vec{F}_z} + \; b \tag{13b}$$

$$\vec{T}_z = \vec{M}_z - (x-a)\vec{F}_y + (y-b)\vec{F}_x \tag{13c}$$

However, the Kistler force plates have a different channel configuration (8-channel configuration) and record data as $\vec{F}_{1Z}$, $\vec{F}_{2Z}$, $\vec{F}_{3Z}$, $\vec{F}_{4Z}$, $\vec{F}_{1x} + \vec{F}_{2X}$, $\vec{F}_{3X} + \vec{F}_{4X}$, $\vec{F}_{1Y} + \vec{F}_{2Y}$, and $\vec{F}_{3Y} + \vec{F}_{4Y}$. Therefore, we needed the location of each of the force sensors relative to the point directly in the center of the plate surface where the coordinates are given as distance from the center point in the X direction (α), distance from the center point in the Y direction (β), and depth from plate surface in the Z direction (γ). α, β, and γ are all given by the manufacturer for each specific Kistler force plate. This is shown in Figure 9.

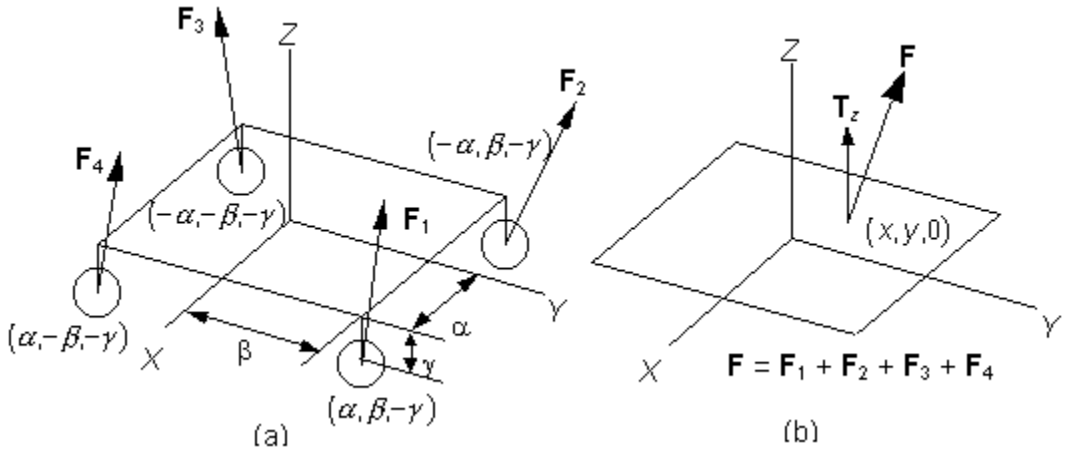

Figure 9. Kistler Force Plate Sensor Configuration. (Kwon, 1998)

Rather than calculating the moments as $\vec{M}_x$, $\vec{M}_y$, and $\vec{M}_z$ as shown in equation (12), the moment for the Kistler force plates is calculated differently where individual moments are calculated at each force sensor, $\vec{M}_1$, $\vec{M}_2$, M_3, and $\vec{M}_4$ as seen in equations (14a), (14b), (14c), and (14d).

$$\vec{M}_1 = [\,\alpha \quad \beta \quad -\gamma] \text{ x } [F_{1x} \quad F_{1y} \quad F_{1z}] = [\beta F_{1z} + \gamma F_{1y} \quad -\gamma F_{1x} - \alpha F_{1z} \quad \alpha F_{1y} - \beta F_{1x}] \qquad (14a)$$

$$\vec{M}_2 = [-\alpha \quad \beta \quad -\gamma] \text{ x } [F_{2x} \quad F_{2y} \quad F_{2z}] = [\beta F_{2z} + \gamma F_{2y} \quad -\gamma F_{2x} + \alpha F_{2z} \quad -\alpha F_{2y} - \beta F_{2x}] \qquad (14b)$$

$$\vec{M}_3 = [-\alpha \quad -\beta \quad -\gamma] \text{ x } [F_{3x} \quad F_{3y} \quad F_{3z}] = [-\beta F_{3z} + \gamma F_{3y} \quad -\gamma F_{3x} + \alpha F_{3z} \quad -\alpha F_{3y} + \beta F_{3x}] \qquad (14c)$$

$$\vec{M}_4 = [\,\alpha \quad -\beta \quad -\gamma] \text{ x } [F_{4x} \quad F_{4y} \quad F_{4z}] = [-\beta F_{4z} + \gamma F_{4y} \quad -\gamma F_{4x} - \alpha F_{4z} \quad \alpha F_{4y} + \beta F_{4x}] \qquad (14d)$$

Using the four equations within equation (14) with our previous computation of center of pressure in equation (13a), (13b), and (13c), we get equation (15).

$$\vec{M} = [M_x \quad M_y \quad M_z] = \vec{M}_1 + \vec{M}_2 + \vec{M}_3 + \vec{M}_4 = [x \quad y \quad 0] \text{ x } [F_x \quad F_y \quad F_z] + [0 \quad 0 \quad T_z] \qquad (15)$$

The cross product on the right side of equation (16) then yields

$$\vec{\mathrm{M}} = [yF_z \quad -xF_y \quad -yF_x + T_z] \tag{16}$$

Furthermore, because we know that

$$\vec{M}_{\mathrm{x}} = \vec{M}_{1\mathrm{x}} + \vec{M}_{2\mathrm{x}} + \vec{M}_{3\mathrm{x}} + \vec{M}_{4\mathrm{x}} \tag{17a}$$

$$\vec{M}_{\mathrm{y}} = \vec{M}_{1\mathrm{y}} + \vec{M}_{2\mathrm{y}} + \vec{M}_{3\mathrm{y}} + \vec{M}_{4\mathrm{y}} \tag{17b}$$

$$\vec{M}_{\mathrm{z}} = \vec{M}_{1\mathrm{z}} + \vec{M}_{2\mathrm{z}} + \vec{M}_{3\mathrm{z}} + \vec{M}_{4\mathrm{z}} \tag{17c}$$

we can create the following equations

$$\vec{M}_{1\mathrm{x}} + \vec{M}_{2\mathrm{x}} + \vec{M}_{3\mathrm{x}} + \vec{M}_{4\mathrm{x}} = \mathrm{y}\vec{F}_{\mathrm{z}} \tag{18a}$$

$$\vec{M}_{1\mathrm{y}} + \vec{M}_{2\mathrm{y}} + \vec{M}_{3\mathrm{y}} + \vec{M}_{4\mathrm{xy}} = -\mathrm{x}\vec{F}_{\mathrm{z}} \tag{18b}$$

$$\vec{M}_{1\mathrm{z}} + \vec{M}_{2\mathrm{z}} + \vec{M}_{3\mathrm{z}} + \vec{M}_{4\mathrm{xz}} = \mathrm{x}\vec{F}_{\mathrm{y}} - \mathrm{y}\vec{F}_{\mathrm{x}} + \vec{T}_{\mathrm{z}} \tag{18c}$$

Finally, plugging the values from equation (14) into the three equations in equation (18) and simplifying, we get the X and Y coordinates of the center pressure as well as $\vec{\boldsymbol{T}}_{\mathbf{z}}$ as shown in equations (19a), (19b), and (19c).

$$x = \frac{\alpha(\vec{F}_{14z} - \vec{F}_{23z}) + \gamma(\vec{F}_{12x} + \vec{F}_{34x})}{F_z} \tag{19a}$$

$$y = \frac{\beta(\vec{F}_{12z} - \vec{F}_{34z}) + \gamma(\vec{F}_{14y} + \vec{F}_{23y})}{\vec{F}_z} \tag{19b}$$

$$\vec{T}_z = \alpha(\vec{F}_{14y} - \vec{F}_{23y}) - \beta(\vec{F}_{12x} - \vec{F}_{23y}) - x(\vec{F}_{14y} + \vec{F}_{23y}) + y(\vec{F}_{12x} + \vec{F}_{34x}) \tag{19c}$$

Knowing α, β and γ, we are now able to calculate the center of pressure from the eight channels of force data recorded by the Kistler force plate.

Next, we needed to correct for the plate padding that was used to make the force plates continuous with the mound. This was done to find the center of pressure at the surface of the

pitching mound rather than force plate surface as calculated above. To do this, we used the method described by Kwon (1998) in which we found the intersection of the vector of the force applied to the plate with the surface of the pad.

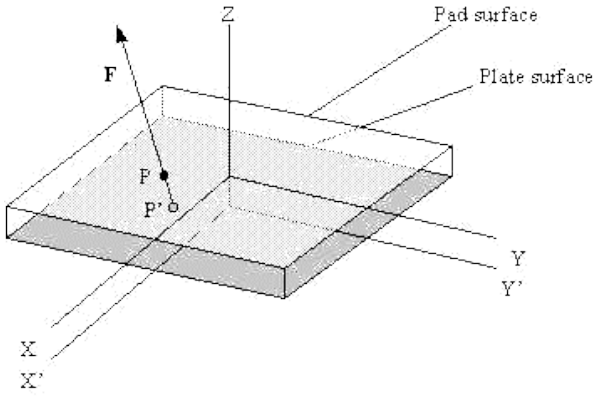

Figure 10. Correction of Center of Pressure for Plate Padding (Kwon, 2008, http://www.kwon3d.com/theory/grf/pad.html)

To begin, we know that point P is the intersection of F and the pad surface. We can then use P to calculate the center of pressure. This does not affect the moment produced by F because P and P' both lie on the line of action of F. If we call the thickness of the pad τ and the unit vector of $\vec{F}$, [n_x , n_y , n_z], then we know

$$k = \tau / \vec{n}_z \tag{20a}$$

$$x = x' + k \cdot \vec{n}_x \tag{20b}$$

$$y = y' + k \cdot \vec{n}_y \tag{20c}$$

where k = a scale constant, (x, y) = the coordinates of point P in the XY system, and (x', y') = the coordinates of point P' in the X'Y'-system. Therefore, (x, y) above are the new CP coordinates to be used in the data analysis. Once corrected for the Kistler plates, we obtain equations (21a) and (21b) where x and y represent the X and Y coordinates of the center of pressure at the plate pad surface.

$$x = \frac{\alpha[(\vec{F}_{1z}+\vec{F}_{4z})-(\vec{F}_{2z}+\vec{F}_{3z})]+(\gamma+\tau)\vec{F}_x}{\vec{F}_z} \tag{21a}$$

$$y = \frac{\beta[(\vec{F}_{1z}+\vec{F}_{2z})-(\vec{F}_{3z}+\vec{F}_{4z})]+(\gamma+\tau)\vec{F}_y}{\vec{F}_z} \tag{21b}$$

The last processing step for the data prior to statistical analysis was correcting the directional differences in forces between left-handed pitchers and right-handed pitchers,

specifically in the X direction. Because the two different types of pitchers (left-handed vs. right-handed) stand in opposite facing directions when pitching the ball, the respective GRF data they generate have opposite values in the X direction. To correct this, the X component of all GRF data for left-handed pitchers was negated as described in equation (8). Effectively, this allowed us to view all pitchers as right-handed pitchers.

Dependent Variables

1. Maximum GRFs were calculated and expressed in an activity relevant reference frame. All GRFs were reported as a percentage of body weight for each pitcher.
2. GRF impulse in the X, Y, and Z directions.
3. Center of pressure location on the mound surface above each plate.
4. Stride length was computed as the distance in the Y direction between the average location of the stride foot CP on the landing plate (plate 2) between the instants of stride foot contact and release and the average location of the push foot CP (plate 1). Stride length was expressed as a percent of each pitcher's standing height.
5. Ball speed in m/s.

Statistics

1. Descriptive statistics were computed using SPSS and Microsoft Excel.
2. Two-way repeated measures ANOVAs were used to determine if there were any statistically significant differences ($p < 0.05$) for each dependent variable based on pitch type, pitch delivery or for pitch x delivery interactions.
3. Correlations were used to examine the relationships between the dependent variables and both ball speed and stride length.

Results and Discussion

No pitch type by pitch delivery interactions were present for any of the variables examined.

Ball Speed

As expected, ball speed ($F[1,7] = 58.575$) was significantly greater in fastballs than changeups (Table 1 and Figure 11). However, there was no significant difference in ball speed for pitch delivery.

Table 1. Mean and Standard Deviation Values for Ball Speed (m/s).

	WU FB	WU CU	ST FB	ST CU	Main Effect Delivery	Main Effect Pitch Type
Ball Speed					$F_{1,7} = 4.589$	$F_{1,7} = 58.575$
M	37.42	33.08	37.09	32.72	$p = .069$	$p = .000$
SD	1.48	2.10	1.36	2.15	$\eta^2 = .396$	$\eta^2 = .893$

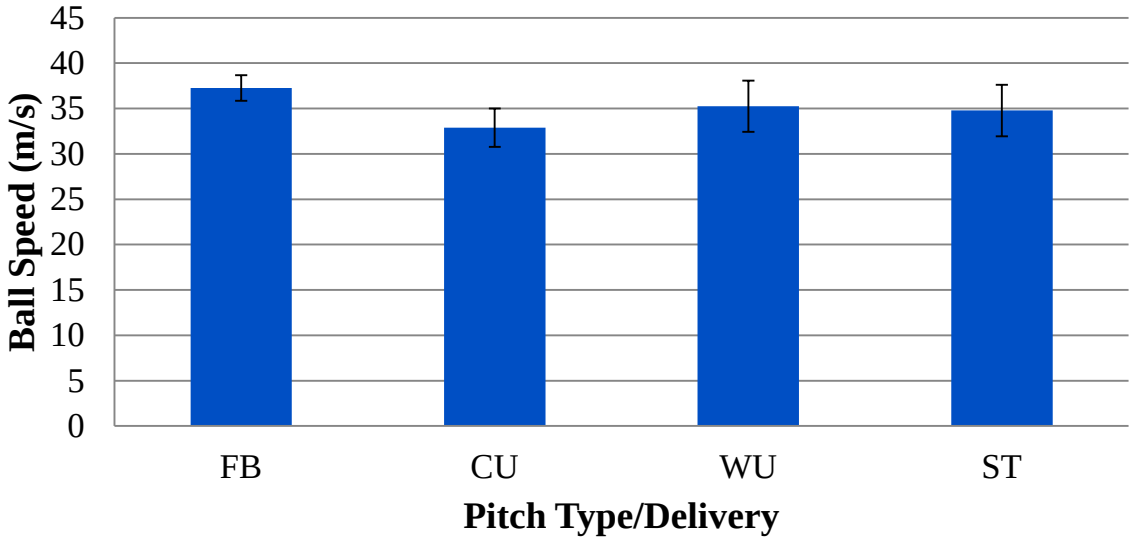

Figure 11. Mean ball speed by pitch type and pitch delivery. Error bars indicated ±1 standard deviation.

It is interesting to see no significant difference between pitch deliveries as it is a commonly held view in the baseball community that the windup delivery allows pitchers to throw with a greater ball velocity in relation to the stretch delivery. With no significant difference between the two delivery types, it may be better to instruct pitchers to throw from the stretch all the time for two main reasons: the stretch delivery is much less complicated to learn and execute and the stretch delivery is required during the most crucial aspects of the game (runners on base). Pitching from the stretch all the time may allow a pitcher to feel more comfortable in this particular delivery. However, future studies are needed to further investigate the kinematic and kinetic differences in angular momentum for pitch delivery in order to gauge the windup's effectiveness compared to the stretch to make a well-supported claim.

Ground Reaction Forces

Before investigating the GRF data findings, examination of representative ground reaction force graphs provides a foundational understanding of the forces exerted on the pitcher during the pitching motion. [Note: exemplar graphs shown in Figures 12 through 19) are all from the same subject.] Figure 12 demonstrates the GRFs of the push foot on the rubber plate during a windup fastball.

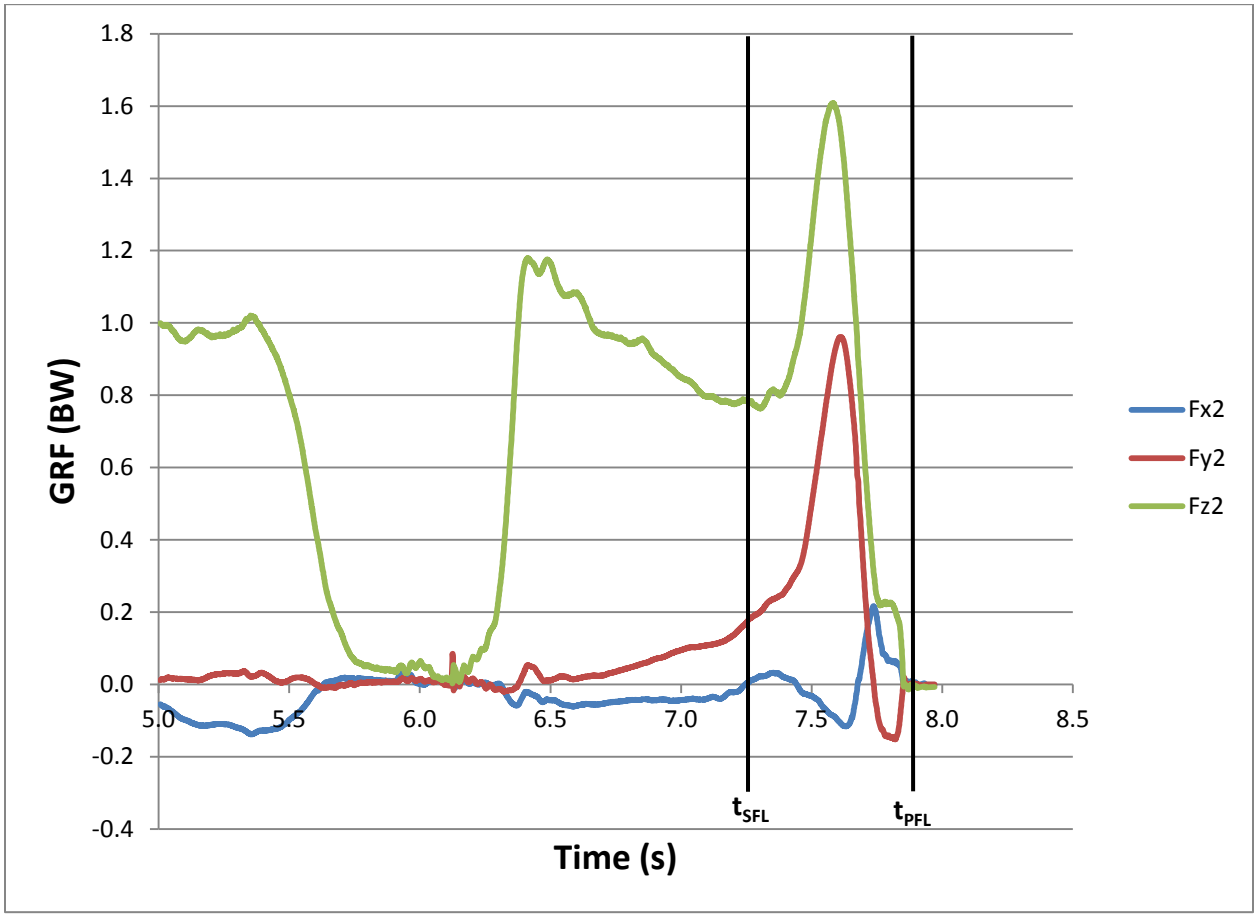

Figure 12. Example graph of GRF data for rubber force plate during a windup fastball.

Where t_{SFL} is the instant of stride foot lift from the rubber plate and t_{PFL} is the instant of push foot lift from the rubber plate. The two instants will be identified in all subsequent graphs for the rubber force plate during a given pitch delivery and pitch type.

In this particular graph, there is a greater variance in the X and Z direction forces compared to the stretch. This occurs as a result of the winding up motions during this particular delivery. Secondly, the Y direction GRFs are larger as a result of the fastball pitch relative to a windup pitch. These differences will be discussed later in the section.

Figure 13 builds off the previous graph by demonstrating the GRFs exerted on the stride foot during a windup fastball.

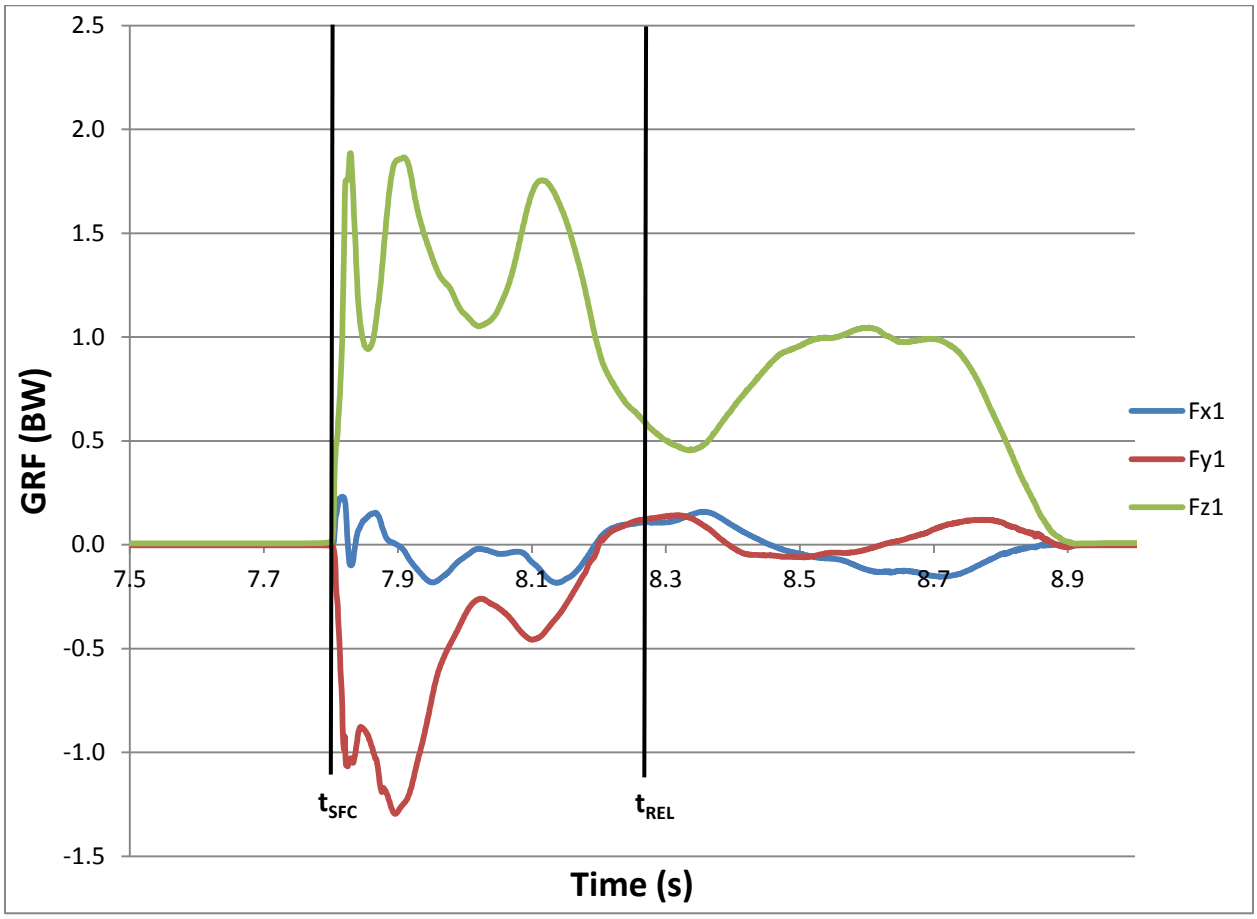

Figure 13. Example graph of GRF data for landing force plate during a windup fastball.

Where t_{SFC} is the instant of stride foot contact with the landing plate and t_{REL} is the instant of ball release. These notations of points in time will be used for all subsequent graphs for the landing plate.

This particular graph shows large negative Y direction GRFs which occur to slow the forward motion of the pitcher. The X direction GRFs are minimal as there is very little change in lateral movement of the pitcher at this point in the pitching motion.

Figure 14 shows an example of the GRFs exerted on the push foot during a fastball thrown from the stretch.

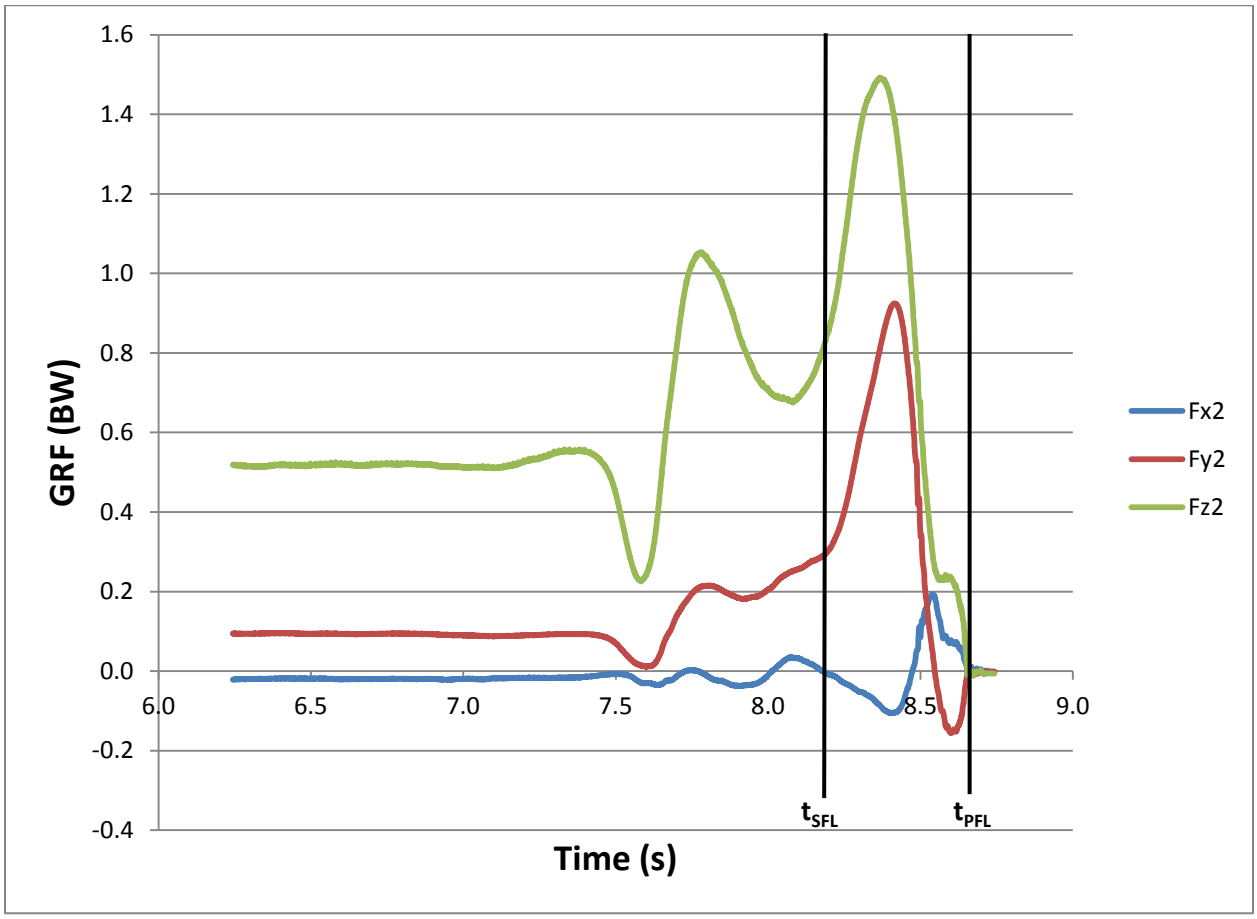

Figure 14. Example graph of GRFs for rubber force plate during a stretch fastball.

The main differences in this graph from Figure 12 are the relatively small changes in the X direction GRFs which occur as a result of the absence of the windup pitching motion. The Y direction GRFs are also greater than what are typically seen in the changeup pitch as shown in Figure 16 and 18. However, the Y direction GRFs were not significantly different for pitch delivery.

Figure 15 shows an example of the GRFs exerted on the stride foot during a fastball thrown from the stretch.

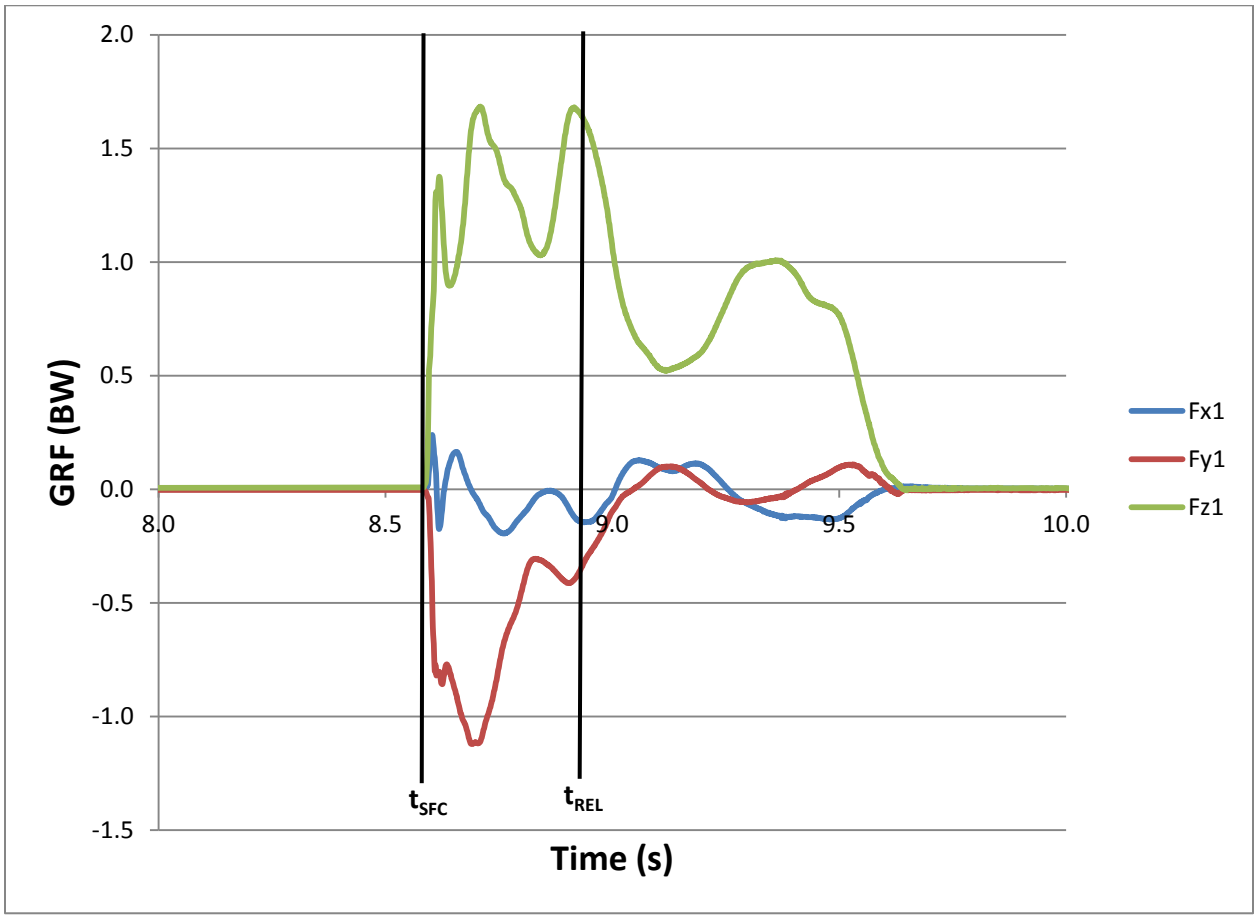

Figure 15. Example graph of GRF data for rubber force plate during a stretch fastball.

Comparing with Figure 13, we see relatively little difference in the GRFs exerted on the stride foot based upon pitch delivery. As mentioned earlier, the GRFs of the stride foot generally don't change significantly for pitch delivery.

Figure 16 demonstrates an exemplar graph of the GRFs exerted on the push foot during a changeup thrown from the windup.

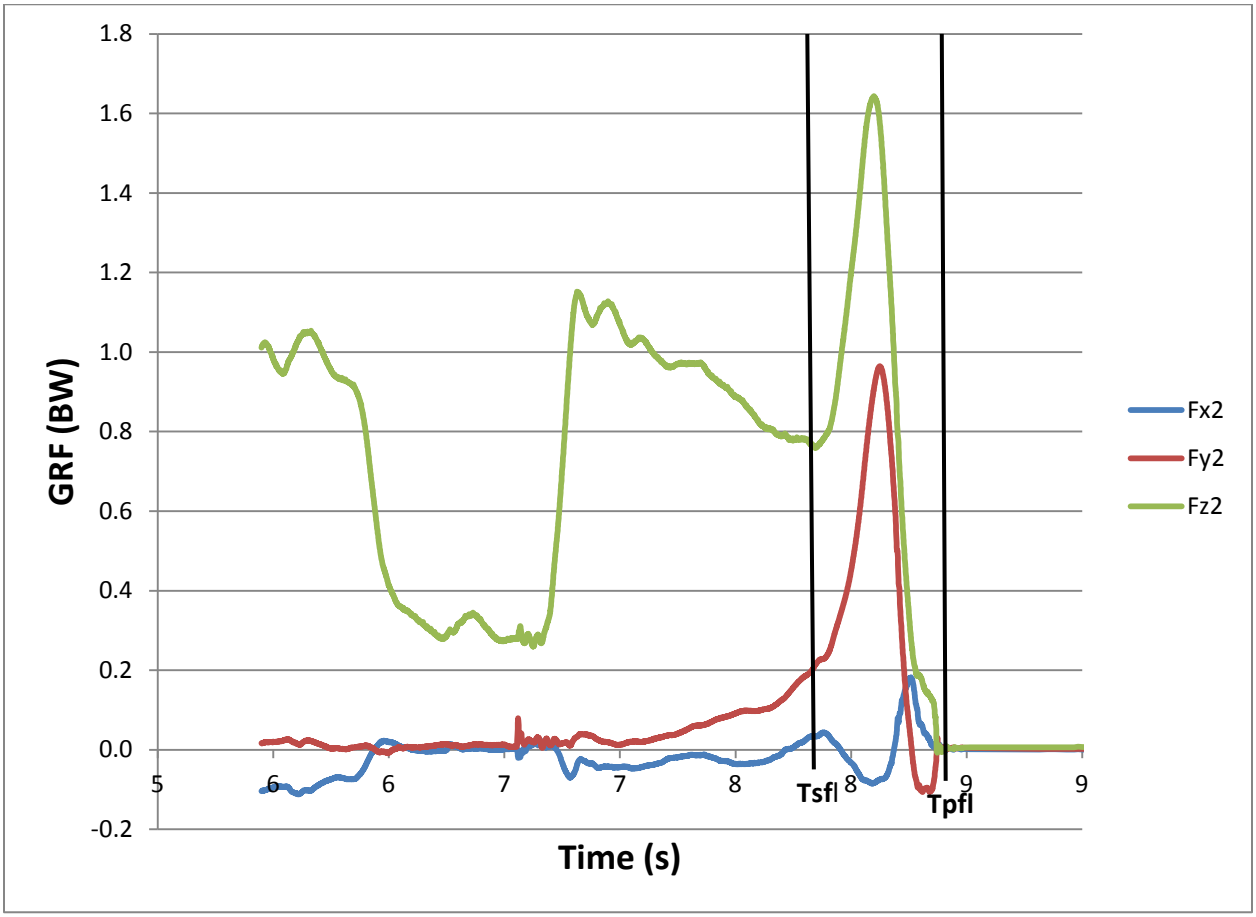

Figure 16. Example graph of GRF data for rubber force plate during a windup changeup.

As seen earlier, the characteristic changes in the X and Z direction GRFs are present due to the windup pitching motion prior to stride foot lift. Because the pitch is a changeup, smaller magnitude positive Y direction GRFs are created in order to produce the desired slower ball speed at release.

Figure 17 exemplifies the GRFs exerted on the stride foot during a changeup thrown from the windup.

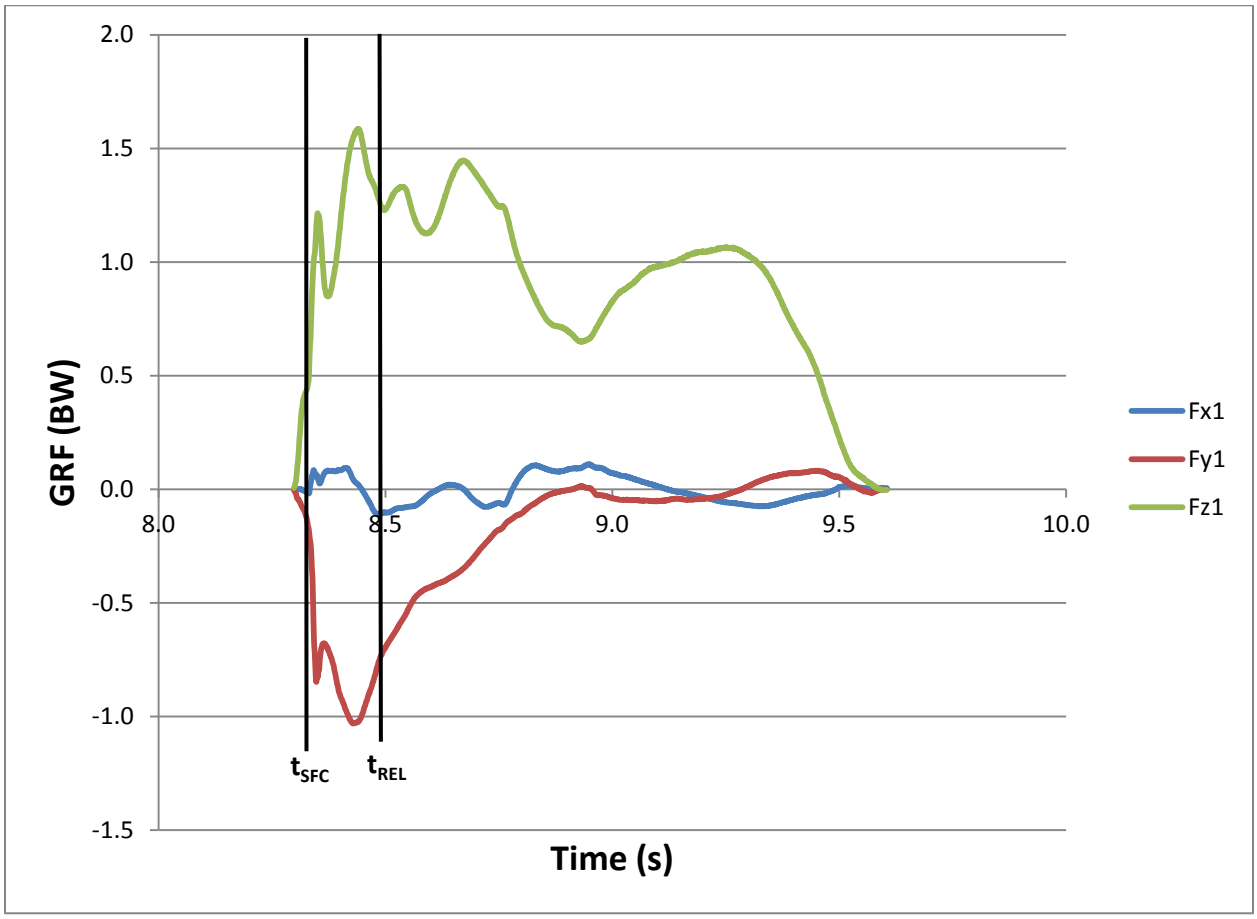

Figure 17. Example graph of GRF data for landing force plate during a windup changeup.

The same general trends from the previous stride foot graphs are seen; however, lesser negative Y direction GRFs occur as a result of the smaller positive Y direction GRFs that occurred in Figure 16.

Figure 18 shows the GRF graph of the push foot for a changeup thrown from the stretch.

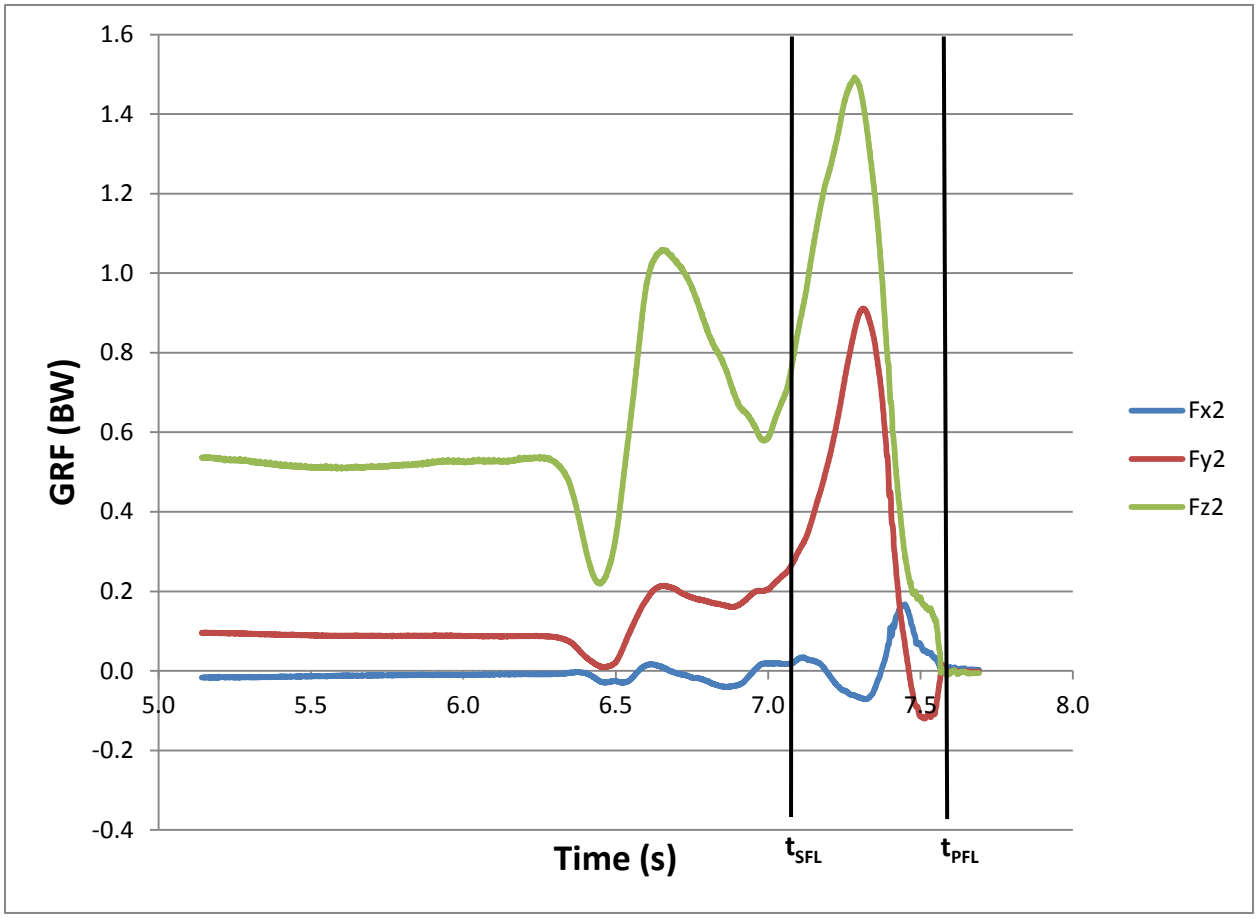

Figure 18. Example graph of GRF data for rubber force plate during a stretch changeup.

The same general trends present in Figure 14 are here as well. This is due to the stretch delivery type being consistent regardless of pitch type. Once again, the positive Y direction GRFs are smaller in order to produce a changeup pitch (lower ball velocity).

Figure 19 shows the GRFs exerted on the stride foot during a changeup thrown from the stretch.

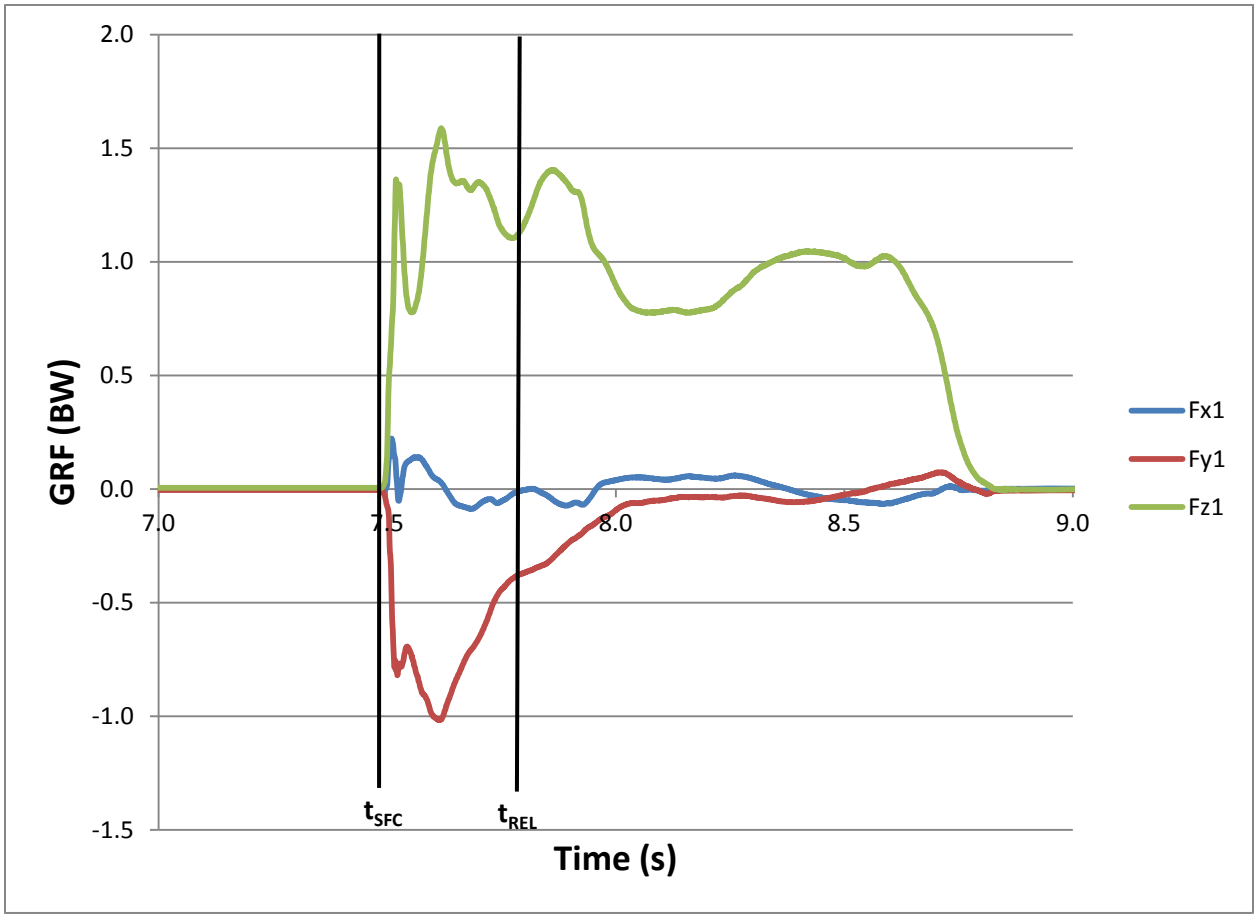

Figure 19. Example graph of GRF data for landing force plate during a stretch changeup.

Looking at the previous GRF graphs for the stride foot, there is very little difference when compared to Figure 19. Once again, in response to the smaller positive Y direction GRFs in the push foot (Figure 18), the negative Y direction GRFs of the stride foot also are smaller.

Analyzing the GRF data for all pitchers, inferences can be made on relationships within the data for pitch type and pitch delivery. Fastballs had greater ($F[1,7] = 5.995$) anteriorly-directed [Y direction] ground reaction forces in the push foot (Table 2, Figure 20). These greater anteriorly-directed forces caused a greater forward motion towards home plate of the pitcher's center of mass, ultimately resulting in an increased ball speed and stride length. Thus, driving harder off the back leg (push foot) allows the pitcher generate a greater forward momentum which is important in maximizing ball velocity.

Table 2. Mean and Standard Deviation Values for Maximum GRFs in the Push Foot.

	WU FB	WU CU	ST FB	ST CU	Main Effect Delivery	Main Effect Pitch Type
Maximum F_X GRF					$F_{1,7} = 17.380$	$F_{1,7} = 2.541$
M	0.14	0.13	0.07	0.07	$p = .004$	$p = .155$
SD	0.03	0.03	0.04	0.02	$\eta^2 = .713$	$\eta^2 = .266$
Maximum F_Y GRF					$F_{1,7} = .071$	$F_{1,7} = 5.995$
M	0.78	0.75	0.78	0.75	$p = .798$	$p = .044$
SD	0.13	0.14	0.13	0.15	$\eta^2 = .010$	$\eta^2 = .461$
Maximum F_Z GRF					$F_{1,7} = 9.276$	$F_{1,7} = 3.551$
M	1.51	1.47	1.45	1.42	$p = .019$	$p = .102$
SD	0.17	0.13	0.20	0.13	$\eta^2 = .570$	$\eta^2 = .337$

GRF values are expressed as a percentage of body weight

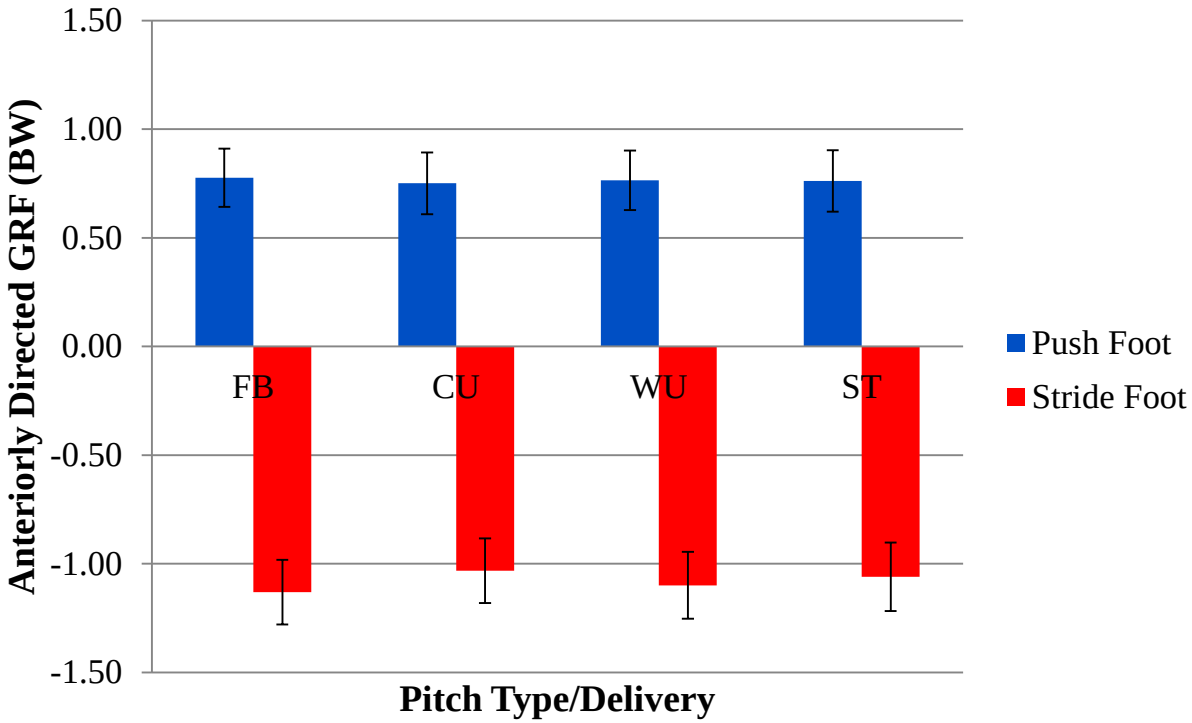

Figure 20 Anteriorly-directed ground reaction forces [+ Y direction] of the push foot and posteriorly-directed ground reaction forces [- Y direction] of the stride foot as a percentage of body weight for pitch type and pitch delivery. Error bars indicate ±1 standard deviation.

Pitcher's throwing from the windup delivery also experienced greater (F[1,7] = 17.38) mediolateral ground reaction forces [X direction] in the push foot directed positively towards the pitching arm (Table 2, Figure 21).

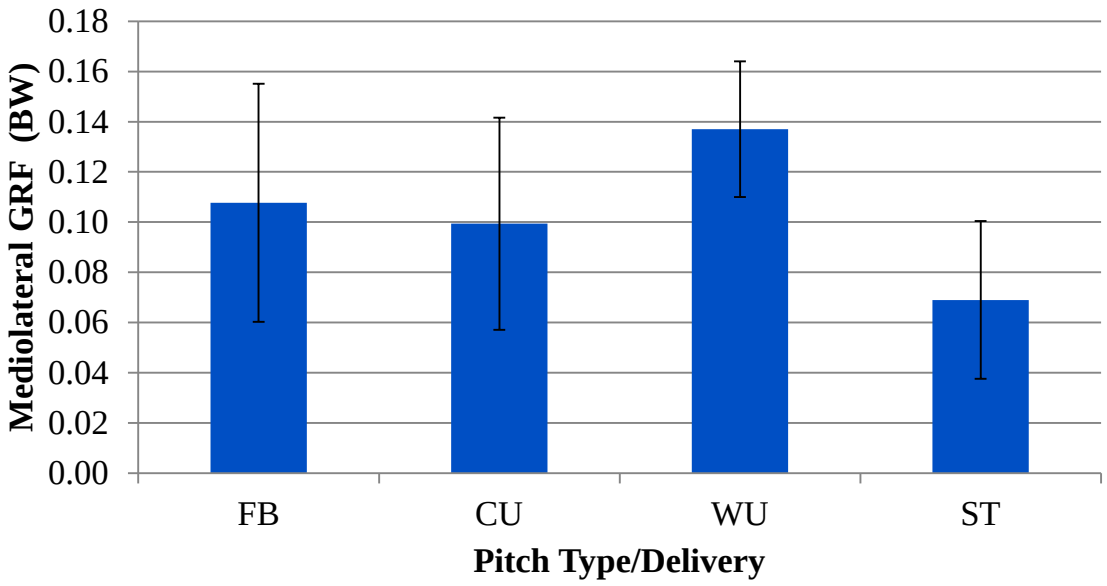

Figure 21 Mediolateral ground reaction forces [X direction] (as a percentage of body weight) in the push foot by pitch type and pitch delivery. Error bars indicate ±1 standard deviation.

These increased forces were likely present to accommodate the increased mediolateral range of motion of the pitcher's center of mass during the windup pitch delivery. This is further confirmed by the much smaller mediolateral GRFs seen in the stretch in which there is a smaller mediolateral range of motion of the pitcher's center of mass.

Windup pitches also exhibited significantly larger maximum Z direction GRFs. The larger GRFs in the Z direction found in windup pitches are likely due to the need for the pitcher to generate larger frictional forces to produce the large magnitude X direction (mediolateral) GRFs.

In order to slow the forward motion generated during the pitch, the pitcher experienced greater ($F[1,7] = 13.103$) posteriorly-directed ground reaction forces [- Y direction] in the stride foot (Table 3, Figure 20) during both windup and fastball pitches. These Y direction forces occurring in the negative Y direction acted as a braking system to allow the pitcher to stabilize the front leg, trunk, and upper body, allowing them to effectively transfer the angular momentum up to body to the hand where it is applied to the ball. Similar to Elliott et. al. (1988), these increased forces allowed the pitcher to drive over a more stabilized stride leg, allowing them to create a greater ball velocity seen in fastballs. It is unclear as to why the larger posteriorly-directed GRFs in windup pitches were not associated with larger ball speeds compared to stretch delivery pitches.

Table 3. Mean and Standard Deviation Values for Maximum GRFs in the Stride Foot.

	WU FB	WU CU	ST FB	ST CU	Main Effect Delivery	Main Effect Pitch Type
Maximum F_X GRF					$F_{1,7} = .417$	$F_{1,7} = .159$
M	0.16	0.15	0.16	0.15	$p = .539$	$p = .702$
SD	0.06	0.05	0.06	0.06	$\eta^2 = .056$	$\eta^2 = .022$
Minimum F_Y GRF					$F_{1,7} = 7.975$	$F_{1,7} = 13.103$
M	-1.14	-1.06	-1.12	-1.01	$p = .026$	$p = .009$
SD	0.15	0.15	0.15	0.14	$\eta^2 = .533$	$\eta^2 = .652$
Maximum F_Z GRF					$F_{1,7} = 8.320$	$F_{1,7} = 12.045$
M	2.02	1.86	1.91	1.79	$p = .023$	$p = .010$
SD	0.34	0.32	0.34	0.31	$\eta^2 = .543$	$\eta^2 = .632$

GRF values are expressed as a percentage of body weight

Both windup and fastball pitches also produced larger magnitude GRFs in the Z direction. As noted in the rubber plate, the larger GRFs in the Z direction are likely due to the need for the pitcher to generate larger frictional forces and produce the larger posteriorly-directed Y direction GRFs.

Impulse

There was a significant difference in the X impulse values for pitch delivery (F[1,7]=89.386) (Table 4) for the push foot. This was an obvious difference as the wind-up motion required greater X direction GRFs in the push foot to compensate for the increased mediolateral range of motion of the pitcher's body as well as a different amount of time over which those forces were applied. There was also a significant difference in the vertical GRFs [Z direction] for pitch delivery (F[1,7]=87.464) (Table 4). The differences in the total Z impulse and the impulse due to weight occurred due to the longer duration of the windup delivery relative to the stretch delivery.

Table 4. Mean and Standard Deviation Values for Impulse in the Push Foot.

	WU FB	WU CU	ST FB	ST CU	Main Effect Delivery	Main Effect Pitch Type
X_{TOTAL} Impulse					$F_{1,7} = 89.386$	$F_{1,7} = 5.009$
M	-0.01	0.01	0.00	-0.01	$p = .000$	$p = .060$
SD	0.01	0.02	0.02	0.03	$\eta^2 = .927$	$\eta^2 = .417$
$X_{POSITIVE}$ Impulse					$F_{1,7} = 58.838$	$F_{1,7} = .004$
M	0.02	0.03	0.03	0.03	$p = .000$	$p = .949$
SD	0.00	0.01	0.02	0.02	$\eta^2 = .894$	$\eta^2 = .001$
$X_{NEGATIVE}$ Impulse					$F_{1,7} = .992$	$F_{1,7} = .992$
M	-0.03	-0.02	-0.02	-0.03	$p = .352$	$p = .352$
SD	0.01	0.01	0.00	0.01	$\eta^2 = .124$	$\eta^2 = .124$
Y_{TOTAL} Impulse					$F_{1,7} = 4.186$	$F_{1,7} = .142$
M	0.26	0.28	0.24	0.26	$p = .080$	$p = .717$
SD	0.02	0.01	0.04	0.01	$\eta^2 = .374$	$\eta^2 = .020$

$Y_{POSITIVE}$ Impulse					$F_{1,7} = 4.007$	$F_{1,7} = 1.375$
M	0.28	0.29	0.25	0.27	$p = .085$	$p = .279$
SD	0.02	0.01	0.04	0.02	$\eta^2 = .364$	$\eta^2 = .164$
$Y_{NEGATIVE}$ Impulse					$F_{1,7} = 2.288$	$F_{1,7} = 12.704$
M	-0.01	-0.01	-0.01	-0.01	$p = .174$	$p = .009$
SD	0.01	0.00	0.00	0.01	$\eta^2 = .246$	$\eta^2 = .645$
Z_{TOTAL} Impulse					$F_{1,7} = 87.464$	$F_{1,7} = .112$
M	1.12	0.98	0.91	1.04	$p = .000$	$p = .748$
SD	0.28	0.17	0.24	0.16	$\eta^2 = .926$	$\eta^2 = .016$
Impulse Duration					$F_{1,7} = 77.606$	$F_{1,7} = .352$
M	1.314	1.315	0.985	0.998	$p = 0.00$	$p = .57$
SD	0.106	0.125	0.136	0.131	$\eta^2 = .92$	$\eta^2 = .05$
Impulse due to Weight					$F_{1,7} = 95.28$	$F_{1,7} = .23$
M	1.27	1.11	1.08	1.19	$p = 0.00$	$p = .64$
SD	0.28	0.17	0.24	0.17	$\eta^2 = .93$	$\eta^2 = .03$

Note. Impulse values are expressed as a percentage of body weight

There were no significant differences for the impulse values in the stride foot for either pitch delivery or pitch type. This was expected as the latter half of the pitching motion (stride foot contact to ball release) does not change significantly based upon pitch delivery or pitch type used.

Table 5. Mean and Standard Deviation Values for Impulse in the Stride Foot.

	WU FB	WU CU	ST FB	ST CU	Main Effect Delivery	Main Effect Pitch Type
X_{TOTAL} Impulse					$F_{1,7} = .058$	$F_{1,7} = .132$
M	0.00	0.01	-0.01	-0.01	$p = .817$	$p = .727$
SD	0.01	0.01	0.01	0.01	$\eta^2 = .008$	$\eta^2 = .019$
$X_{POSITIVE}$ Impulse					$F_{1,7} = 1.20$	$F_{1,7} = 1.44$
M	0.01	0.01	0.00	0.00	$p = .31$	$p = .27$
SD	0.00	0.01	0.00	0.00	$\eta^2 = .15$	$\eta^2 = .17$
$X_{NEGATIVE}$ Impulse					$F_{1,7} = .61$	$F_{1,7} = .67$
M	-0.01	0.00	-0.01	-0.01	$p = .46$	$p = .44$
SD	0.01	0.00	0.00	0.01	$\eta^2 = .08$	$\eta^2 = .09$
Y_{TOTAL} Impulse					$F_{1,7} = .32$	$F_{1,7} = 1.37$
M	-0.12	-0.12	-0.11	-0.10	$p = .591$	$p = .279$
SD	0.02	0.02	0.02	0.02	$\eta^2 = .043$	$\eta^2 = .164$
$Y_{POSITIVE}$ Impulse					$F_{1,7} = 2.50$	$F_{1,7} = .14$
M	0.00	0.00	0.00	0.00	$p = .16$	$p = .72$
SD	0.00	0.00	0.00	0.00	$\eta^2 = .26$	$\eta^2 = .02$
$Y_{NEGATIVE}$ Impulse					$F_{1,7} = .42$	$F_{1,7} = 1.23$
M	-0.12	-0.12	-0.11	-0.10	$p = .54$	$p = .31$

SD	0.02	0.02	0.02	0.02	$\eta^2 = .06$	$\eta^2 = .15$
Z_{TOTAL} Impulse					$F_{1,7} = .734$	$F_{1,7} = .430$
M	0.17	0.18	0.18	0.15	$p = .420$	$p = .533$
SD	0.02	0.03	0.04	0.04	$\eta^2 = .095$	$\eta^2 = .058$
Time Impulse					$F_{1,7} = 3.80$	$F_{1,7} = 1.45$
M	0.00	0.00	0.00	0.00	$p = .09$	$p = .27$
SD	0.00	0.00	0.00	0.00	$\eta^2 = .35$	$\eta^2 = .17$
Impulse due to Weight					$F_{1,7} = .53$	$F_{1,7} = 1.43$
M	0.15	0.18	0.17	0.13	$p = .49$	$p = .27$
SD	0.02	0.02	0.03	0.02	$\eta^2 = .07$	$\eta^2 = .27$

Impulse values are expressed as a percentage of body weight

Center of Pressure

Figure 22 shows the X and Y coordinates of the CP relative to the midpoint of the front edge of the pitching rubber (coordinates 0, 0) over the time interval from about 1.5s prior to stride foot lift until push foot lift.

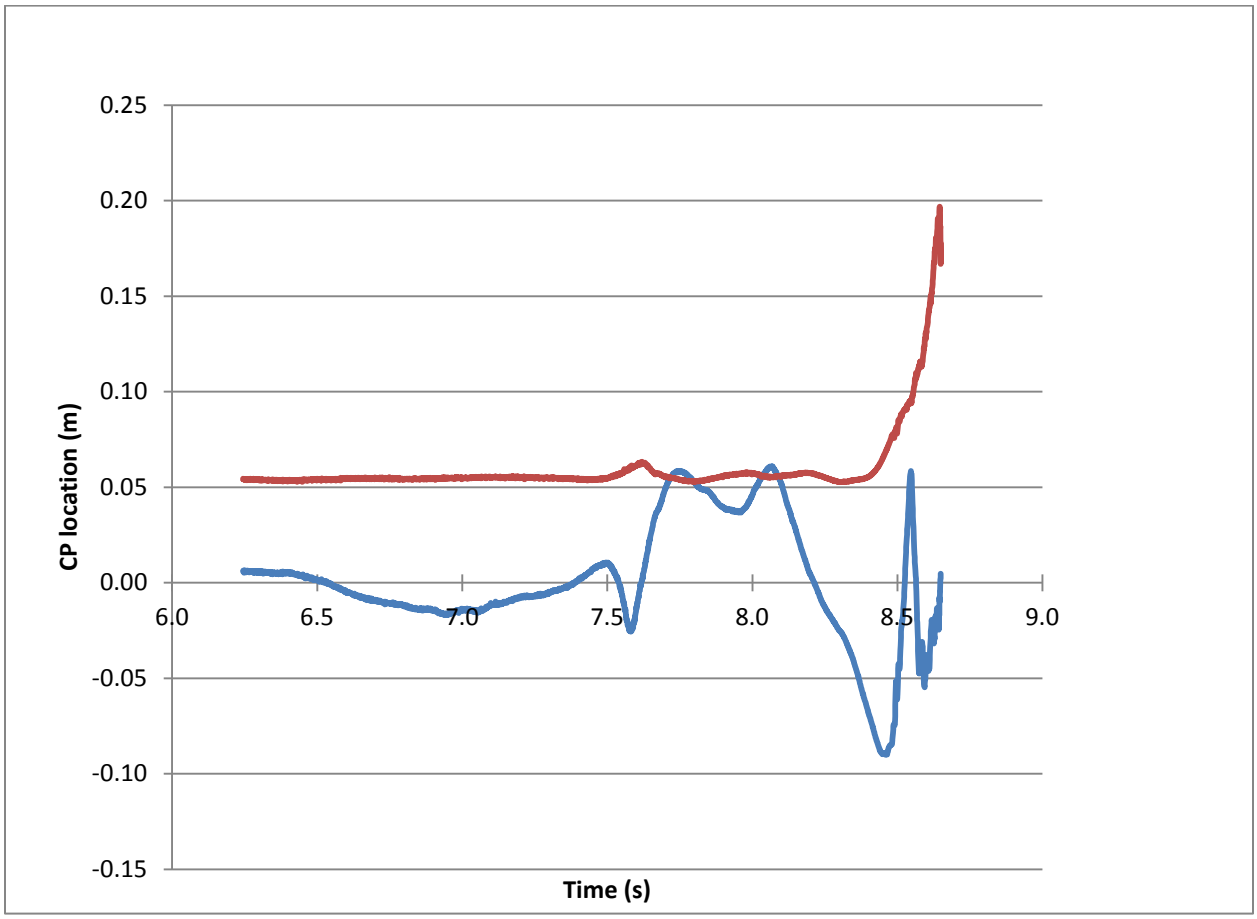

Figure 22. Center of Pressure location (Blue = X Coordinate, Red = Y Coordinate) versus time for the Rubber Plate.

A more activity-relevant graph (Figure 23) was created to demonstrate the translation of the center of pressure data throughout the pitch. Each data point on the Y coordinate (m) vs. X coordinate (m) graph represents the position of the CP relative to the rubber (pink rectangle). Presented in this format, position of the pitcher's push foot CP during the first half of the pitching motion (1.5 seconds prior to stride foot lift through push foot lift) is easily visualized.

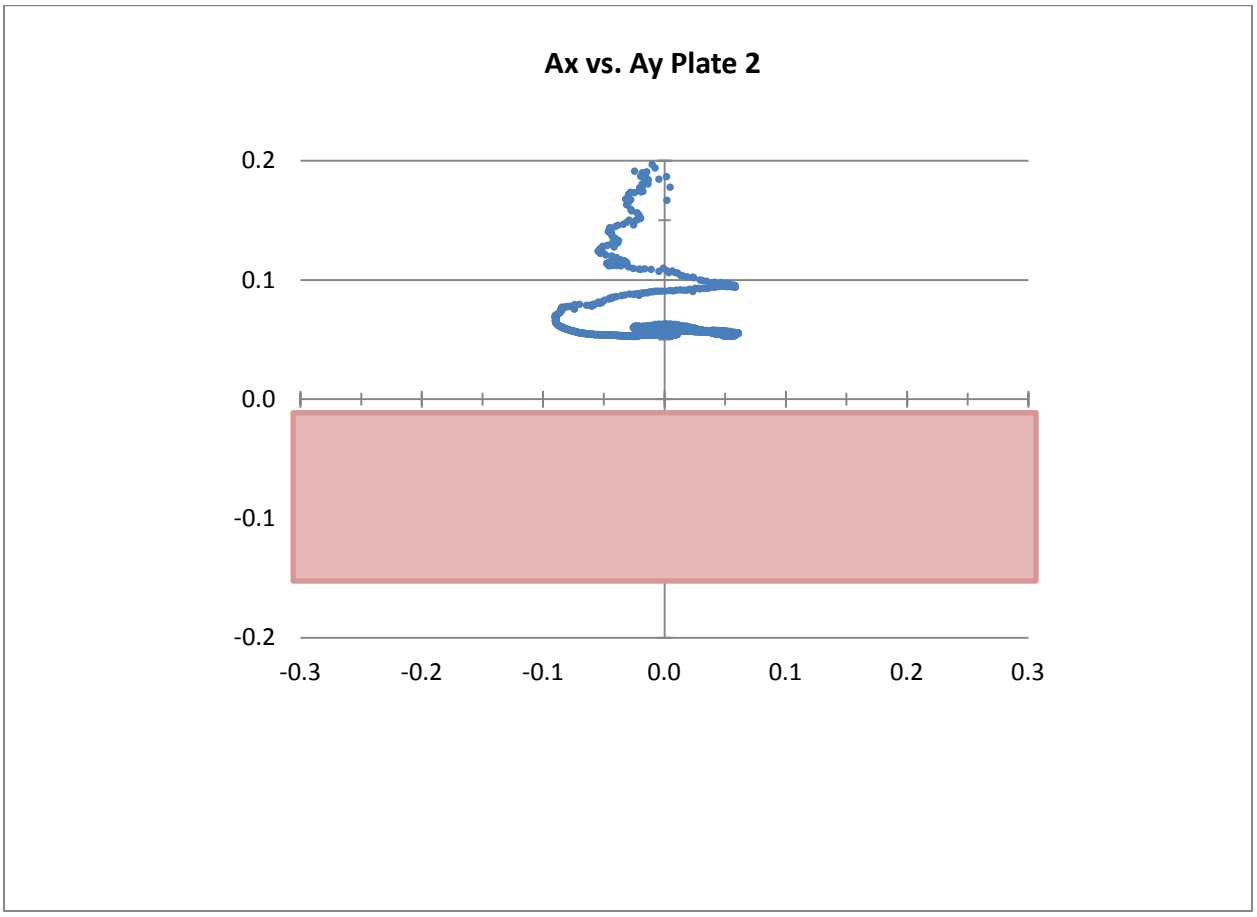

Figure 23. Center of pressure path for the push foot.

Figure 24 displays the X and Y coordinates of the CP relative to the center of the landing plate (coordinates 0, 0) for the stride foot.

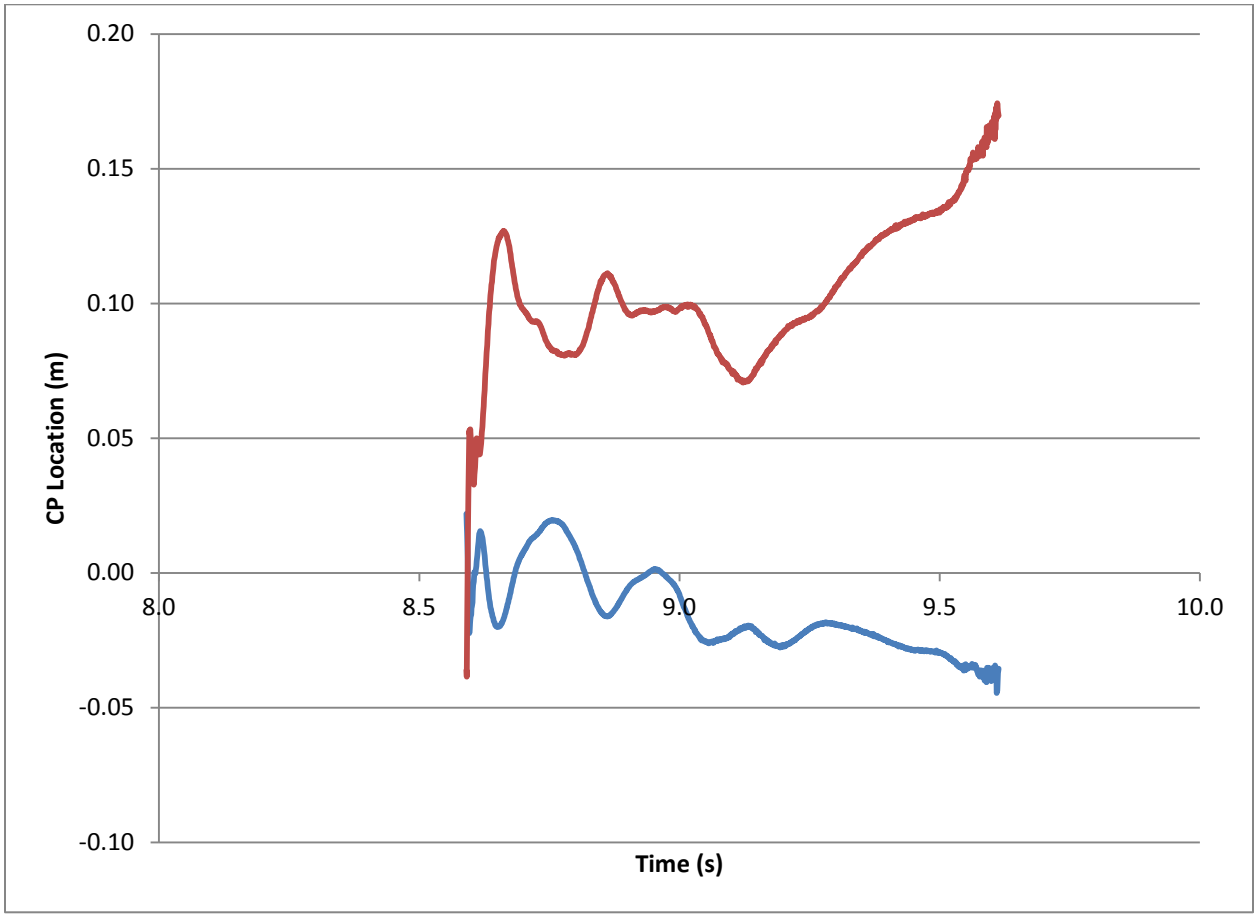

Figure 24. Center of Pressure locations (Blue = X Coordinate, Red = Y Coordinate) versus time for the Landing Plate.

Figure 25 uses the data from the previous graph (Figure 24) and displays the path of the CP relative to the center of the landing plate (coordinates 0, 0).

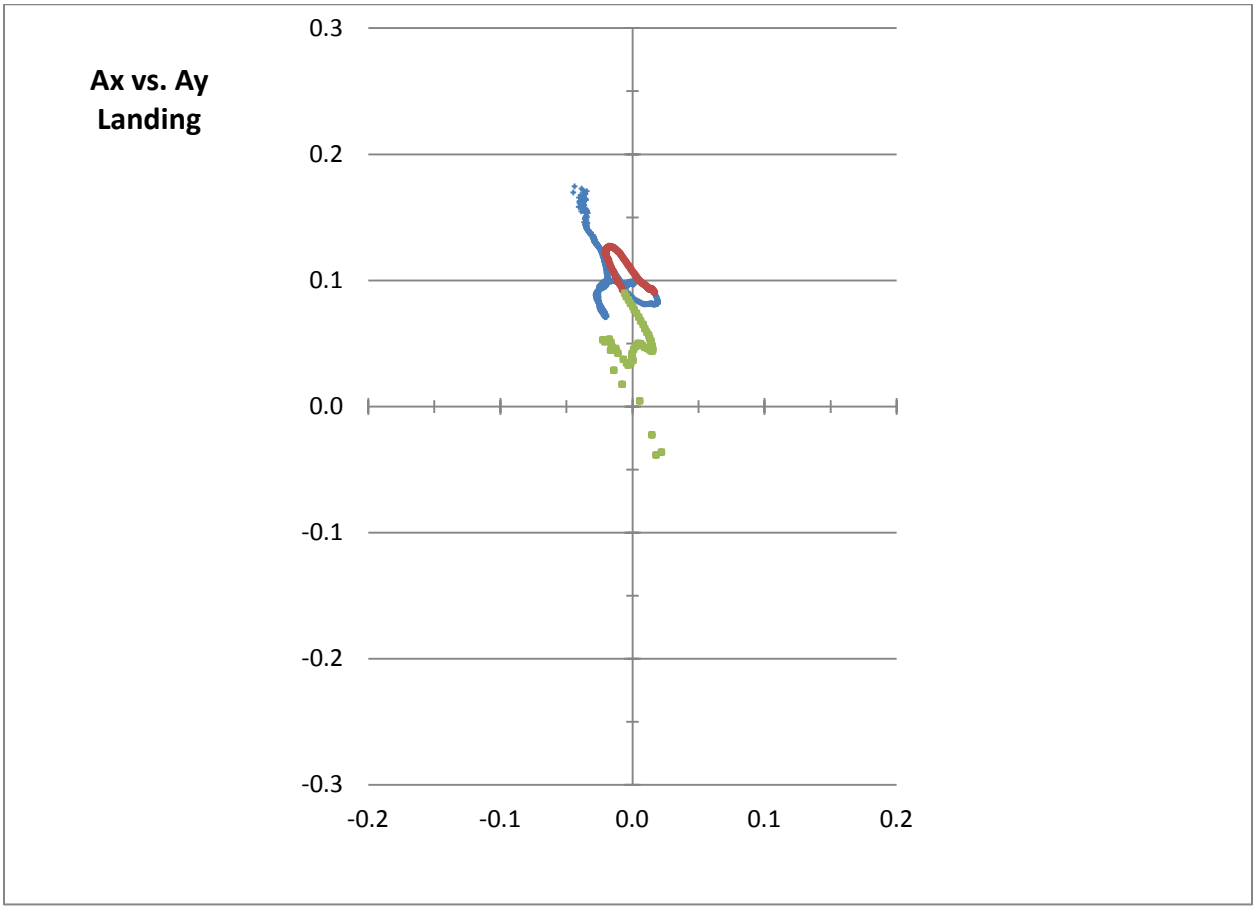

Figure 25. Center of pressure path for the stride foot. The green circles represent the locations of the CP during the initial 50 ms following stride foot landing. The red circles represent the path of the CP for the period from 50 ms following landing through ball release. The blue circles show the path of the CP following ball release.

Stride Length

Stride length was significantly greater (F[1,7] = 18.053) in the windup delivery than the stretch but did not differ based on pitch type (Table 6 and Figure 26).

Table 6. Mean and Standard Deviation Values for Stride Length.

	WU FB	WU CU	ST FB	ST CU	Main Effect Delivery	Main Effect Pitch Type
Stride Length (m)					$F_{1,7} = 18.053$	$F_{1,7} = 1.273$
M	1.68	1.68	1.66	1.65	$p = .004$	$p = .296$
SD	0.05	0.06	0.05	0.07	$\eta^2 = .721$	$\eta^2 = .154$
Stride Length (%)[a]					$F_{1,7} = 18.085$	$F_{1,7} = 1.676$
M	0.90	0.89	0.88	0.87	$p = .004$	$p = .237$
SD	0.03	0.03	0.03	0.04	$\eta^2 = .721$	$\eta^2 = .193$

[a] Stride length values are expressed as a percentage of standing height

Because there was no significant difference in the anteriorly-directed ground reaction forces of the push foot for pitch delivery, the increased stride length seen in the windup delivery (Figure 20) may be due to a different kinematic trajectory caused by the windup motion. However, without kinematic data, there is no way to determine the direct cause of this increased stride length for the windup.

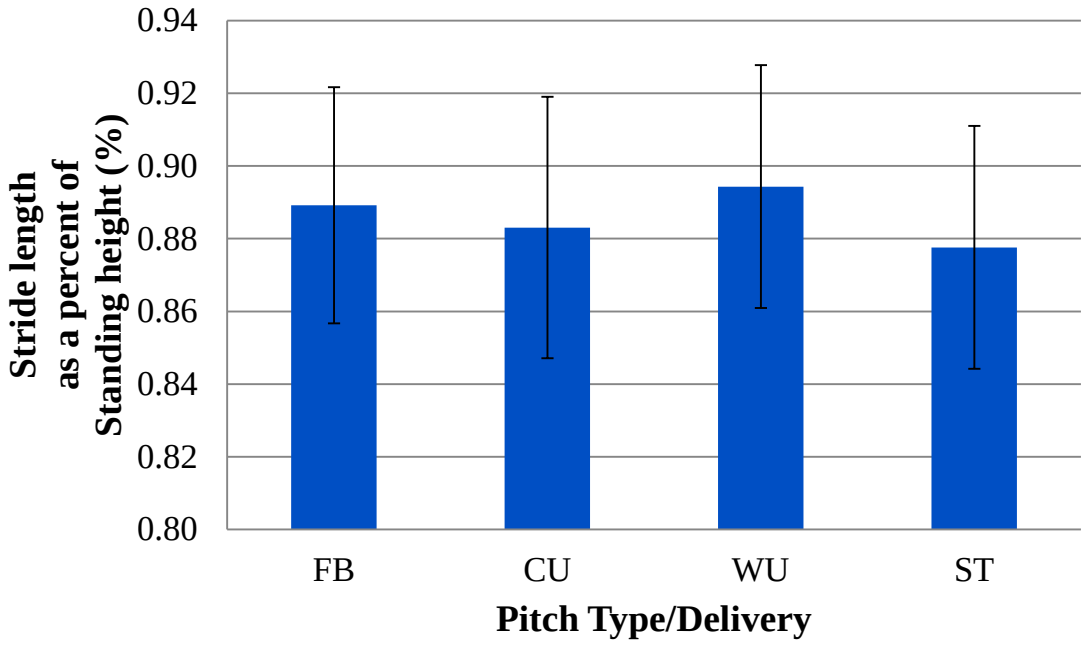

Figure 26. Stride length (as a percentage of standing height) by pitch type and pitch delivery. Error bars indicate ±1 standard deviation.

Correlational Analysis

Ball speed had a strong positive correlation with stride length in fastballs (Table 7 and Table 8) regardless of the type of pitch delivery. This was believed to be due to greater anteriorly-directed ground reaction forces in the push foot resulting in a larger ball speed at release. Thus, driving harder off the push foot resulted in a faster pitch. There was also a strong negative correlation of ball speed with vertical ground reaction forces in the stride foot (Table 7) in all changeup pitches regardless of the type of delivery. Pitchers who landed with greater vertical forces in the stride foot were able to effectively slow down their change-up, a desired trait for this pitch. This could be useful as it would allow the pitcher to throw an effective changeup without tipping the hitter by changing his pitching mechanics [Note: The 3 cm decrease in stride length from fastball to changeup (Table 6 and Figure 26) is likely impossible to detect by a hitter at any level and would not be considered a significant change in pitching mechanics]. In the future, the collection of kinematic data with kinetics could lead to a better understanding of how a greater vertical ground reaction force in the stride foot is directly related to a decreased ball velocity.

Table 7. Significant Correlations (r > 0.5) with Ball Speed.

	WU FB	WU CU	ST FB	ST CU
Stride Length (%)	0.56	-	0.52	-
Push Maximum F_Y (BW)	-	-	-	0.54
Stride Maximum F_Z (BW)	-	-0.54	-	-0.60

*p < 0.05 for all | r >0.5 |

Table 8. Significant Correlations (r > 0.5) with Stride Length (%).

	WU FB	WU CU	ST FB	ST CU
Ball Speed	0.56	-		-
Push Maximum F_Y (BW)	0.73	0.67	0.78	0.69

*p < 0.05 for all | r >0.5 |

There was also a strong positive correlation with anteriorly-directed ground reaction forces for all pitches (Table 8). Thus, driving harder off the push foot is likely to result in an increase in stride length. Stride length was also correlated with ball speed in the fastball pitch (r = 0.56). As mentioned early, this is believed to be due to increased anteriorly-directed ground reaction forces that occur in the fastball pitch (Figure 20).

Summary

As discussed previously, the overhand pitching motion is known to require a transfer of angular momentum from the legs, through the trunk and ultimately to the throwing arm (Lin, 2003). This angular momentum is generated from the pitcher's lower limbs and thus the ground reaction forces exerted on the pitcher are vital in the overhand throwing motion. The results of this study were similar to those reported by MacWilliams et. al. (1998) in that pitchers used the anteriorly directed ground reaction forces [+ Y direction] of the push foot to generate a forward motion of their body. After planting the stride foot, the pitchers generated posteriorly directed ground reaction forces [- Y direction] in the stride foot to help slow their forward motion. However, because highly skilled pitchers were used in this study, the ground reaction forces

relative to the pitcher's body weight were much greater than that of MacWilliams et. al. (1998). Pitchers throwing from the windup also generated greater mediolateral ground reaction forces [X direction] in the push foot to help compensate for the increased mediolateral range of motion that occurs during the windup pitching motion.

These increased ground reaction forces ultimately were correlated with an increased ball speed and an increased stride length which is logical from a kinematic standpoint. Based upon this data and previous studies, the leg drive plays an important role in baseball pitching. Pitchers should be instructed on how to properly use their lower limbs, especially the push foot, to drive off the mound in order to create maximum ball velocity. Areas of instruction may include strength training of the lower limbs, timing of the lower limb drive (Elliott, 1988), and correct mechanics of the pitching motion, all of which will help facilitate an optimal transfer of these ground reaction forces up the body to the ball.

Limitations

The primary limitation of this study was the laboratory dimensions. There was only about 22 feet between the pitching rubber and the lab wall due to space constraints. Therefore, pitchers threw into a net about 20 feet away from the rubber rather than to catcher positioned 60.5 feet from the rubber and in accordance with Major League baseball standards. Because of this setup, there was no way to determine whether each analyzed pitch was a ball or a strike.

Conclusions

1. Fastballs, regardless of delivery type, resulted in a greater ball speed.

2. Increased ball speed likely resulted from increased anteriorly directed ground reaction forces of the push foot which then caused increased posteriorly directed ground reaction forces of the stride foot to slow the pitcher's forward motion after ball release.

3. Increased anteriorly directed ground reaction forces also resulted in an increased stride length regardless of pitch delivery or pitch type.

4. A greater mediolateral range of motion of the pitcher's center of mass during the windup delivery resulted in increased mediolateral ground reaction forces in the push foot.

References

Allison, K. (2008). Joba Chamberlain pitching in 2008 [Online image]. Retrieved May 16, 2012. http://fr.wikipedia.org/wiki/Fichier:Joba_Chamberlain_pitching_2008.jpg.

Atwater, A. E. (1970). Movement characteristics of the overarm throw: A kinematic analysis of men and women performers (Vol. 1). University of Wisconsin--Madison.

Atwater, A. E. (1979). Biomechanics of overarm throwing movements and of throwing injuries. Exercise & Sport Sciences Reviews, (7), 43-85.

Bales, A. (2007). Pitching sequence of David Riske [Online image]. Retrieved May 16, 2012. (http://en.wikipedia.org/wiki/File:Evolution_of_a_Pitch_DavidRiske.jpg)

Dillman, C. J., Fleisig, G. S., & Andrews, J. R. (1993). Biomechanics of pitching with emphasis upon shoulder kinematics. Journal of Orthopaedic & Sports Physical Therapy, 18(2), 402-408.

Elliott, B., Grove, J. R., & Gibson, B. (1988). Timing of the lower limb drive and throwing limb movement in baseball pitching. International Journal of Sports Biomechanics, 4(1), 59-67.

Feltner, M., & Dapena, J. (1986). Dynamics of the Shoulder and Elbow Joints of the Throwing Arm During a Baseball Pitch. International Journal of Sport Biomechanics, 2(4), 235-259.

Fleisig, G. S., Dillman, C. J., & Andrews, J. R. (1989). Proper mechanics for baseball pitching. Clinical Journal of Sports Medicine, 1(1), 151-170.

Kistler (2012). Kistler force plate formulae. Retrieved May 16, 2012. (http://www.health.uottawa.ca/biomech/courses/apa6905/kistler.pdf).

Kwon, Y. H. (1998). Center of pressure: (GRF application point). Retrieved from http://www.kwon3d.com/theory/grf/cop.html

Kwon, Y. H. (1998). Center of pressure: Plate padding. Retrieved from http://www.kwon3d.com/theory/grf/pad.html

Lin, H-T., Su, F-C., Nakamura, M, & Chao, E Y.S. (2003). Complex chain of momentum transfer of body segments in the baseball pitching motion. Journal of the Chinese Institute of Engineers, 26(6), 861-868.

MacWilliams, B A., Choi, T., Perezous, M K., Edmund, Y.S. C., & McFarland, E G. (1998). Characteristic ground-reaction forces in baseball pitching. American Journal of Sports Medicine, 26(66).

Phaeron. (2010). VirtualDub (Version 1.9.11) [Computer software]. Retrieved May 16, 2012. (http://www.virtualdub.org/)

Wesikopf, D. Pitching sequence of Don Sutton [Online image]. Retrieved May 16, 2012. http://www.baseballplayamerica.com/skills/sutton_seq2_2011.jpg